geosciences

MDPI

Article

Upper Jurassic–Lower Cretaceous Source Rocks in the North of Western Siberia: Comprehensive Geochemical Characterization and Reconstruction of Paleo-Sedimentation Conditions

Evgeniya Leushina [1,*], Timur Bulatov [1], Elena Kozlova [1], Ivan Panchenko [2], Andrey Voropaev [3], Tagir Karamov [1], Yakov Yermakov [1], Natalia Bogdanovich [1] and Mikhail Spasennykh [1]

[1] Skolkovo Institute of Science and Technology, Territory of Innovation Center "Skolkovo", Bolshoy Boulevard 30, Bld. 1, 121205 Moscow, Russia; timur.bulatov@skoltech.ru (T.B.); e.kozlova@skoltech.ru (E.K.); tagir.karamov@skoltech.ru (T.K.); yakov.yermakov@skoltech.ru (Y.Y.); n.bogdanovich@skoltech.ru (N.B.); m.spasennykh@skoltech.ru (M.S.)
[2] MIMGO, Entuziastov Highway 21, 111123 Moscow, Russia; ivpanchenko89@gmail.com
[3] HYDROISOTOP GmbH, Woelkestr. 9, 85301 Schweitenkirchen, Germany; AV@Hydroisotop.de
* Correspondence: e.leushina@skoltech.ru

Abstract: The present work is devoted to geochemical studies of the Bazhenov Formation in the north of the West Siberian Petroleum Basin. The object is the Upper Jurassic–Lower Cretaceous section, characterized by significant variations in total organic carbon content and petroleum generation potential of organic matter at the beginning of the oil window. The manuscript presents the integration of isotopic and geochemical analyses aimed at the evaluation of the genesis of the rocks in the peripheral part of the Bazhenov Sea and reconstruction of paleoenvironments that controlled the accumulation of organic matter in sediments, its composition and diagenetic alterations. According to the obtained data, the sediments were accumulated under marine conditions with a generally moderate and periodically increasing terrigenous influx. The variations in organic matter composition are determined by redox conditions and terrigenous input which correlate with the eustatic sea level changes during transgressive/regressive cycles and activation of currents. Transgression is associated with an intensive accumulation of organic matter under anoxic to euxinic conditions and insignificant influence of terrigenous sources, resulting in the formation of rocks with oil-generating properties. During the regression periods, the terrigenous sedimentation increased along with the dissolved oxygen concentration, and deposits with low organic matter content and gas-generating properties were formed.

Keywords: organic matter; sedimentation conditions; paleoenvironment; source rock; pyro-GCxGC-MS; isotope composition; trace elements; the Bazhenov Formation

check for updates

Citation: Leushina, E.; Bulatov, T.; Kozlova, E.; Panchenko, I.; Voropaev, A.; Karamov, T.; Yermakov, Y.; Bogdanovich, N.; Spasennykh, M. Upper Jurassic–Lower Cretaceous Source Rocks in the North of Western Siberia: Comprehensive Geochemical Characterization and Reconstruction of Paleo-Sedimentation Conditions. *Geosciences* **2021**, *11*, 320. https://doi.org/10.3390/geosciences11080320

Academic Editors: Jesus Martinez-Frias, Ronald W. Klusman and Suzanne Golding

Received: 25 May 2021
Accepted: 26 July 2021
Published: 30 July 2021

Publisher's Note: MDPI stays neutral with regard to jurisdictional claims in published maps and institutional affiliations.

Copyright: © 2021 by the authors. Licensee MDPI, Basel, Switzerland. This article is an open access article distributed under the terms and conditions of the Creative Commons Attribution (CC BY) license (https://creativecommons.org/licenses/by/4.0/).

1. Introduction

The Bazhenov Shale Formation of the West Siberian Petroleum Basin is one of the world's largest hydrocarbon (HC) reservoirs, and in recent decades it has attracted attention as an unconventional hydrocarbon source. The oil and gas production in the region is accompanied by the expansion of the fundamental knowledge on the genesis of the Bazhenov Formation, which is the main oil source of the Basin.

According to different estimations, the epicontinental Bazhenov Sea in the Upper Jurassic period occupied an area of up to 2 million km^2 [1,2], and its northern part was connected to the Boreal Sea through a relatively narrow channel [3]. Differences in sedimentation conditions and initial organic matter type in the central and peripheral areas led to the formation of the Bazhenov deposits with different lithological characteristics, total organic carbon (TOC) distribution, composition, and petroleum generation potential. The results of the studies of the Bazhenov Formation rocks and organic matter are reported in numerous publications, including the marine sediments of the central part (distal areas of

the paleo-sea) [1,4–9] and sediments formed in the peripheral parts (proximal paleo-sea areas) [1,5,7,10–14]. Although data have been extensively published, there is still a potential for deepening the knowledge via application of the scope of analytical methods and investigation of the least studied areas.

The northern Bazhenov Formation is one of the least studied and explored regions of the Basin [15]. The majority of the works are devoted to the origin of the gas of the giant gas fields in the region [11,12,16–19], and the detailed vertical variations of the composition and genesis of the deposits are reported in a few studies [14,20–22].

The present study is devoted to the investigation of the Bazhenov section in the northern part of Western Siberia; the core samples were collected from one well drilled in the area between the Yamal and the Gydan regions. The interval investigated includes the Bazhenov Formation and upper part of the Abalak Formation deposits from the Oxfordian stage of the Upper Jurassic to the Berriasian of the Lower Cretaceous (Figure 1).

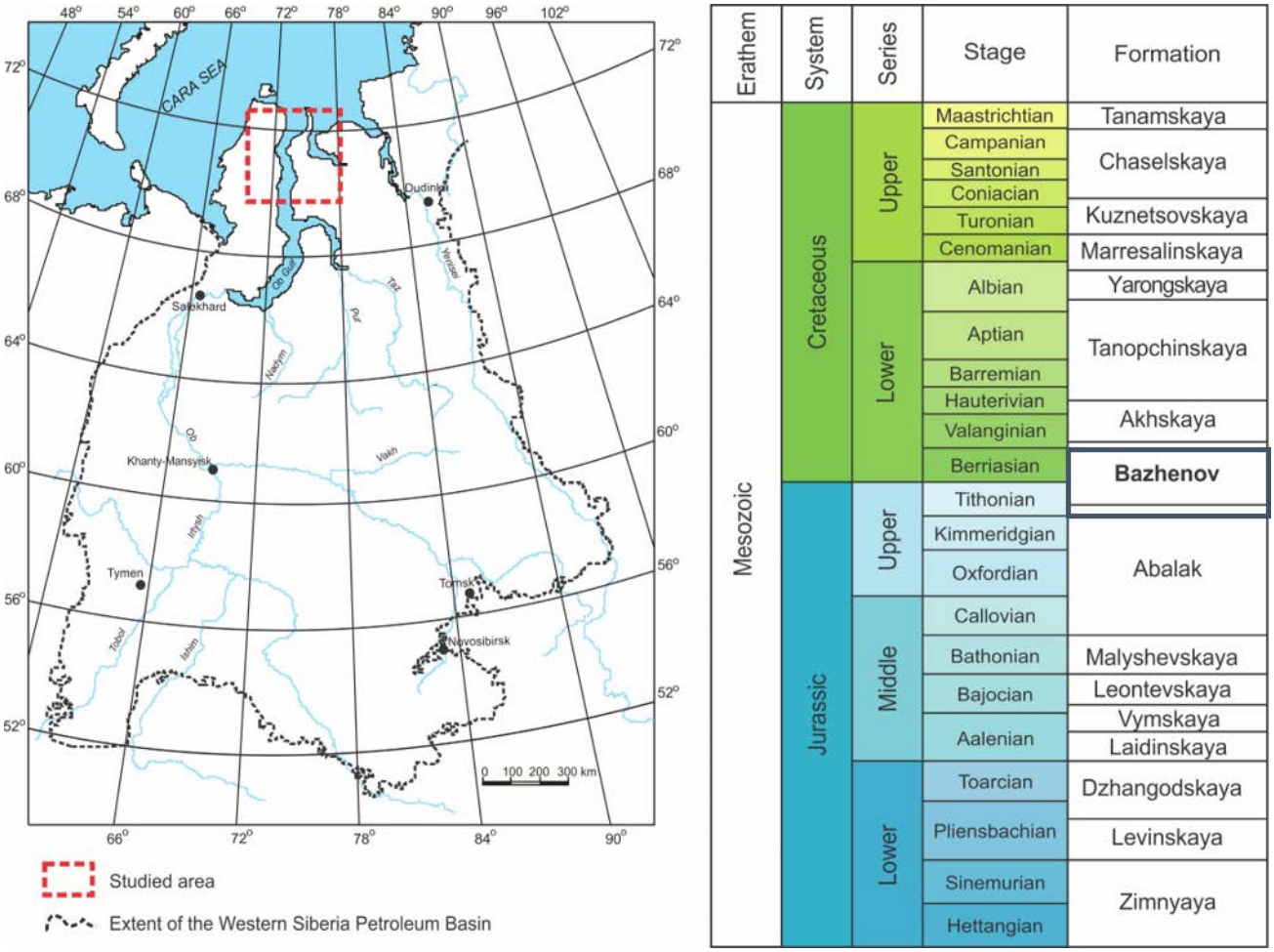


Figure 1. Location of the studied area (modified after Zanin [4]) and stratigraphy of Mesozoic deposits (modified after Afanasenkov [14]); the investigated stratigraphic interval is marked by frame.

Since the area was located at the border between the Bazhenov epicontinental and the Boreal Seas, the deposits were formed under frequently changing depositional conditions and the continuous influence of terrigenous influx. The sequence consists of alternating darker colored organic-rich and lighter organic-poor deposits, that differ from the Bazhenov Formation rocks of the central part of the Basin [13,23]. The mineral composition of rocks is characterized by high clay content, low carbonate content, and significant TOC variations.

The primary focus of this study is to investigate the key features of the different intervals, their genesis and to perform reconstruction of the sedimentation conditions. The

conclusions are based on the results of a number of geochemical and isotope analyses of organic and inorganic components of the rocks. We also investigated the relationships between paleo-sedimentation conditions and the present characteristics of the rocks and organic matter, which determine the prospects for oil and gas production in the region.

2. Geological Setting

The Bazhenov Formation is Upper Jurassic–Lower Cretaceous organic-rich shale, which mainly consists of biogenic silicites with clay components and carbonate admixture [24]. The Formation has an area of almost the whole of the West Siberian Basin, and is considered the major source rock in the region [1,25]. Siliceous mudstones of the Formation were deposited in the sea basin during the Tithonian–Lower Valanginian in the deep water depression in the territory of modern western Siberia (Figure 1). The average thickness of the deposits varies between 20 and 50 m. The Bazhenov source rocks are underlayed by Abalak Formation (Callovian-Lower Tithonian) clay deposits also containing shale, carbonate rocks formed in shallow seas [26,27].

The Bazhenov Formation and its stratigraphic equivalents formed in the distal parts of the paleo-sea consist of siliceous rocks enriched in organic matter that accumulated under anoxic marine conditions. Similar depositional conditions were present over the central part of the Basin, whereas the marginal paleo-sea areas were influenced by terrigenous influx and sea-level alterations. Therefore, the rocks in the central part of the Bazhenov are lithologically homogeneous over the large territory and form the largest oil shale formation in the world, both in thickness and area. Despite the high amount of organic matter in the deposits, no large oil fields are found in its central part due to the low permeability of rocks and preservation of liquid hydrocarbons in its pore space. The productive intervals are thus attributed to porous and fractured carbonates or diagenetic carbonates in radiolarites, which contain low amounts of syngenetic organic matter (kerogen and/or asphaltenes) [28]. During recent years, the Bazhenov Formation has been considered not only as a source rock but also as an unconventional reservoir. In contrast, the deposits in the peripheral parts were accumulated under the influence of various factors including the river and periodical flows, tectonic setting, connection with ocean waters, etc. Therefore, the deposits formed in the peripheral paleo-sea areas are depleted in organic matter and have higher terrigenous material and clay mineral content compared to that of the central part of the Basin.

The area investigated is located in the northern part of the West Siberian Basin close to the Arctic region. In terms of tectonics, the area is in the Yamal-Gydan megasaddle, at the boundary between the Yamal and Gydan regions (Figure 1). There are widely known gas and oil fields in the region, such as Stormovoe, Gydanskoye, Salmanovskoye, and Tambeyskoye, and the Bazhenov Formation is considered the main source rock [17].

3. Samples and Methods

In the current study, a core from 1 well was examined, using a varying number of samples according to the applied technique. Details are given in the corresponding sections of the results.

The lithological study was performed at different scales, from core description to optical microscopy and scanning electron microscopy (SEM).

Optical microscopy was performed with polarizing microscope AxioScope 5 (Carl Zeiss, Jena, Germany) on specially prepared thin sections with thickness 10–20 μm for better mudrock fabric recognition [29].

For the detailed study of micromorphological rock features, scanning electron microscopy (SEM) was used. Quattro S (Thermo Fisher Scientific, Waltham, MA USA) allowed us to analyze small (3–5 mm) rock samples with an electron beam current range from 1 pA to 200 nA with an accelerating voltage of 5 to 10 kV. Samples were coated with a thin (10 nm) gold layer to discharge samples.

Spectral gamma-ray logging of full-size core was performed on the USGC-1 gamma-ray spectrometer instrument. The vertical resolution was 5 cm.

The chemical composition of rocks was studied by X-ray fluorescence (XRF) using a portable X-MET 8000 Expert Geo spectrometer (Oxford Instruments Analytical GmbH, Uedem, Germany). The core samples were preliminary powdered. Determinations were made according to the settings of a universal calibration program used for a wide range of diagnostic chemical elements (from Mg to U), with a duration of 60 s. As a result, the quantitative analysis of petrogenic chemical elements (Mg, Al, Si, P, S, K, Ca, Ti, Mn, Fe) and of some trace elements (V, Ni, Cu, Zn, Rb, Sr, Zr, Mo, Ba, Th, U, etc.) was performed. This approach allows one to perform the continuous profiling of chemical composition along the interval, obtaining a large amount of geological data without special sample preparation and with an accuracy comparable with individual sample measurements (XRF, ICP-MS, carbonate content measurements). The obtained trends are reliable, since the maxima and minima found are consistent with stationary XRF and ICP-MS measurements performed for individual samples [30].

For Sm, Nd content and isotope ratio measurements, 20–30 mg of rock was crushed and dissolved in the mixture of concentrated acids HF and HNO_3 (5:1, 1 mL). According to the isotope dilution method, the tracer amount was calculated and added. The insoluble organic residue was additionally washed with concentrated HNO_3 and evaporated. The dilution with concentrated HCl and evaporation was repeated three times to obtain the solid matter, containing elements in the form of chlorides. The sample was then dissolved in 2.2 N HCl, and the insoluble residue was removed by centrifugation. The separation of Sm and Nd for isotope composition analysis was carried out by ion-exchange column chromatography. Isotope composition was measured using the "Triton" thermal ionization mass spectrometer (ThermoFisher Scientific, Waltham, MA, USA). To calculate the systematic error and normalize the obtained values, La Jolla standard was used, to identify the degree of contamination of a blank sample with a tracer was analyzed. The obtained $^{143}Nd/^{144}Nd$ ratios were corrected to the age of sedimentation (~145 Ma) using the formula:

$$\left(\frac{^{143}Nd}{^{144}Nd}\right)_i = \frac{^{143}Nd}{^{144}Nd} - \frac{^{147}Sm}{^{144}Nd} * (exp(\lambda t) - 1), \quad (1)$$

where $\left(\frac{^{143}Nd}{^{144}Nd}\right)_i$ is the Nd isotope composition at time t, λ is the decay constant, and $\frac{^{143}Nd}{^{144}Nd}$ and $\frac{^{147}Sm}{^{144}Nd}$ are measured isotope ratios.

Source rock characterization and TOC measurements was carried out using HAWK Resource Workstation (Wildcat Technologies, Humble, Texas, USA) according to the Rock-Eval bulk rock procedure [31,32]. We determined the main pyrolysis parameters: S0, S1, S2, S3, S4, S5, temperature Tmax (°C), and calculated the values of total organic carbon (TOC, wt.%), generative organic carbon (GOC, wt.%) and non-generative organic carbon (NGOC, wt.%), Kgoc (GOC/TOC, %), hydrogen index (HI, mg HC/g TOC), oxygen index (OI, mg CO_2/g TOC), index of productivity (PI), and carbonate carbon content (CC, wt.%).

The bulk kinetic studies of kerogen thermal decomposition were performed using the HAWK Resource Workstation. An extracted rock sample was subjected to non-isothermal pyrolysis at temperatures from 300 to 650 °C at three constant heating rates (3, 10, 30 °C/min) for calculation of kinetic parameters: frequency factor A and activation energy distribution. Hydrocarbon products were transferred from the oven to FID by a constant helium flow (50 mL/min). The obtained pyrograms were computed to discrete activation energy distributions using KINETICS2015 software version 6.020 (GeoIsoChem Corporation) for a fixed frequency factor A = 1×10^{14} s^{-1}.

For Pyro(TD)-GC×GC-TOFMS/FID analysis, a powdered rock sample was placed in a quartz glass vial with a closed round end with a plug of quartz wool. Analyses were carried out using Pegasus 4D (LECO Corporation, St. Joseph, MI, USA) equipped with the pyrolysis injection unit (TDU2 and PYRO, Gerstel). The temperature of thermal extraction was 350 °C, and pyrolysis was performed at 500 °C. For thermal extraction analysis, the distribution of *n*-alkanes and a set of biomarker parameters were calculated,

and for kerogen decomposition products, the temperature 500 °C and exposure time of 30 s were chosen and the main outcome was organic class distribution (Figure 2).

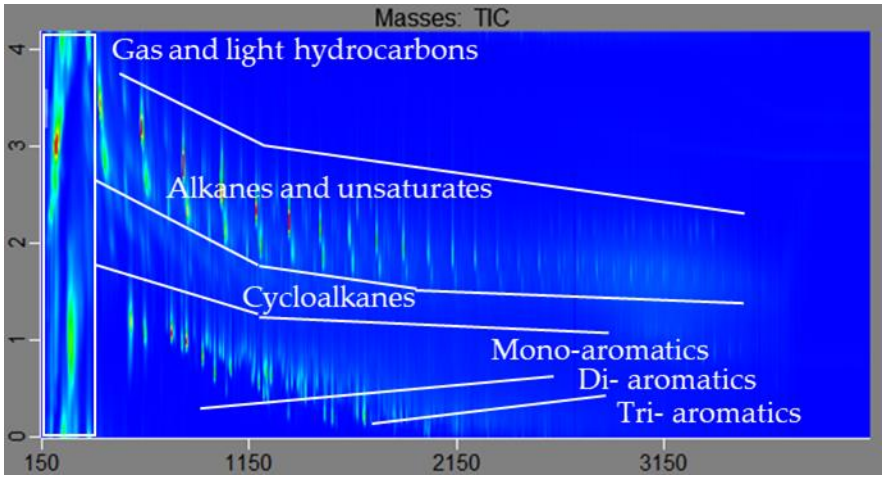


Figure 2. An example of processing a two-dimensional TIC chromatogram for the calculation of organic compound class distribution in pyro-GCxGC-FID/TOFMS.

Two-dimensional gas chromatography was performed using reverse column configuration: Rxi-17Sil MS 30 m and Rxi-5HT 1.5 m (Restek). Helium was used as the carrier gas at a flow rate of 1.4 mL/min. The oven temperature program started from 40 °C then ramped to 340 °C. Two detectors operated simultaneously with 150 s delay. TOFMS electron ionization mode was at 70 eV, the ion source temperature was 250 °C, the voltage was 1600 V, the acquisition rate was 100 Hz and the mass range was 35–450 amu. The FID operation temperature was 350 °C, and the FID acquisition rate was 100 Hz. Data acquisition and processing were carried out using ChromaTOF™ software version 4.70.7.0 (LECO Corporation) and MS Office 2013. Individual component identification was based on the comparison of analysis results with the NIST database and literature data [33–35].

For elemental and isotope composition, DELTA V Plus mass spectrometer (Thermo) equipped with a Flash 2000 elemental analyzer was applied for isotope and elemental analysis of carbon, nitrogen, and sulfur. The accuracy of analytical procedures was established using international standards: oil NBS 22, strontium carbonate NBS 23, ammonium sulfate IAEA-*N*-2, and barium sulfate NBS 127 for carbon, nitrogen, and sulfur, respectively, as well as of the laboratory standards, whose elemental and isotope composition was determined during interlaboratory comparative measurements. The content and isotope composition of organic carbon (C_{org}) and carbonate carbon (C_{carb}) were analyzed separately. The carbon and oxygen isotope composition of carbonates ($\delta^{13}C_{carb}$ and $\delta^{18}O_{carb}$) were analyzed in gaseous CO_2 released during the decomposition of carbonates after 100% orthophosphoric acid treatment. The amount of CO_2 was quantified to obtain C_{carb} content. The residual solution was filtered and the residue containing $C_{org.}$ was analyzed with elemental analyzer using the combustion method. The relative error of element content measurements is ±10%. The measured C, H, N, and S isotopic ratios were recalculated and given in δ values in ‰, giving the deviation of the measured isotopic ratio relative to the isotopic ratio of the corresponding standard: PDB for carbon, SMOW for hydrogen and oxygen, AIR for nitrogen and CDT for sulfur. The absolute error of measurement for δ values was ±0.3 ‰ for carbon, and ±0.5 ‰ for sulfur and nitrogen.

4. Results and Discussion

This section presents the data on various inorganic and organic geochemical analyses: the description of the experimental results and their interpretation based on the published data related to the technique and object of the study. The final subsection is devoted to the integration of the various geochemical data and the reconstruction of sedimentation

conditions to explain the alteration of rock composition, TOC distribution, and hydrocarbon generation potential within the studied section.

4.1. Lithological Description

The samples are composed of argillaceous-siliceous rocks and argillites. The texture is pelitic, cryptocrystalline, and microcrystalline. The rocks have a relatively homogeneous mineral composition, mainly composed of clay minerals (average volume fraction is 42%) and of siliceous components (38% on average). The presence of feldspars (up to 10%), finely dispersed pyrite (up to 8%, in the form of framboids and pseudomorphs on organogenic detritus), and carbonates (mostly lower than 3%, with the exception of three layers with more than 40% carbonate) in the form of calcite and dolomite is detected. Little poorly preserved organogenic detritus of various origin is present (foraminifera shells, radiolarians, and bivalve mollusks).

Since rocks are characterized by relatively stable mineral composition, the main lithological types were distinguished according to rock texture and structure (Figure 3). All established lithological types should be classified as argillaceous-siliceous mudstone according to the classification for fine-grained sedimentary rocks proposed by Lazar et al. [36].

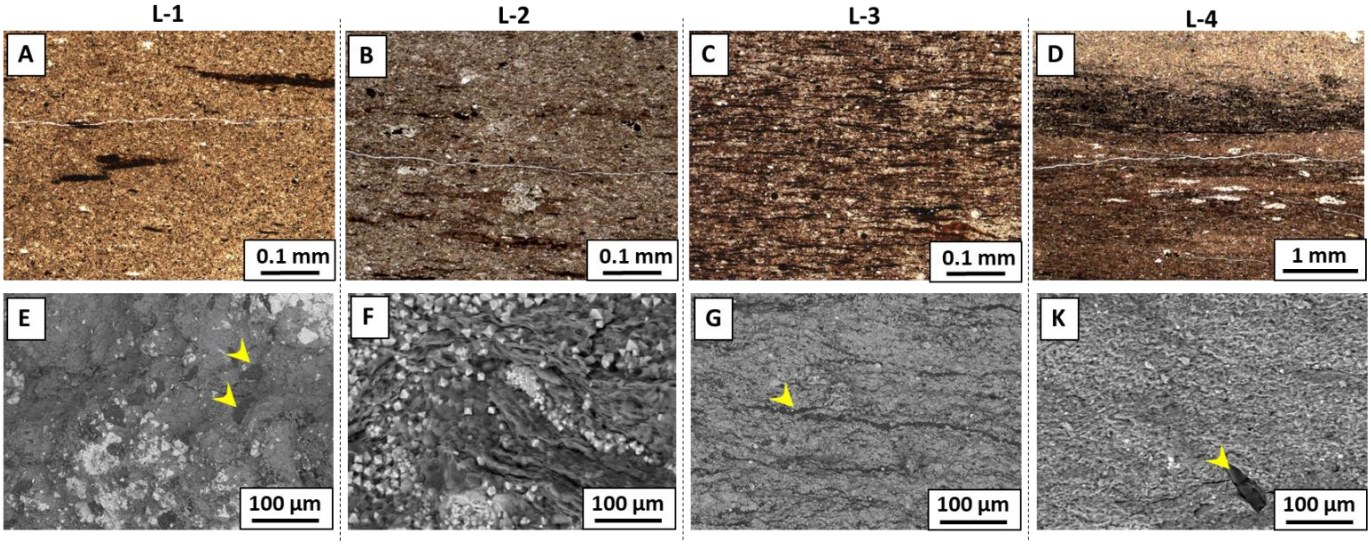


Figure 3. Main lithotypes presented in the studied section: (**A**–**D**)—thin-section images, (**E**–**G**,**K**)—SEM images. Arrows indicate organic matter, two lithotypes are characterized by the lenticular distribution of organic matter in rock (L-2, L-3), and L-1, L-4 show patchy distribution with minor lenticular organic matter.

- Argillaceous-siliceous massive mudstone with bioturbation (L-1): The rocks are bioturbated, and often pyritized. The average TOC content according to pyrolysis data is 2–3 wt.%.
- Argillaceous-siliceous indistinctly laminated mudstone (L-2): Rocks without pronounced lamination at the micro- and macroscopic levels. The average TOC content is 4–5 wt.%.
- Argillaceous-siliceous organic-rich mudstone with planar microscale lamination (L-3): A distinctive feature is a pronounced thin lamination, detected only by microscope and coming from the layer-by-layer distribution of organic matter, clay minerals, and siliceous components. The average TOC content is 7–8 wt.%.
- Argillaceous-siliceous mudstone with thin interlayering of organic-rich and organic-poor laminas and rare bioturbation (L-4): The rocks are characterized by rhythmic formationtal lamination due to the presence of dark gray (enriched in organic matter) and light gray layers, as well as bioturbation. The average TOC content is 2 wt.%.

For the investigated samples, the rock structure is related to organic matter particles shape, orientation and distribution, and its volume fraction is 1–10%. According to our

results, L-3 is characterized by a strong dominance of thin laminas and lenticular inclusions of kerogen (Figure 3C,G), whereas other lithological types host tiny dispersed or patchy organic matter, with a minor role of lenticular inclusions (Figure 3). Variations of organic matter shape cause differences in petrophysical properties of rocks, such as mechanical anisotropy, wettability [37], and many others. Different structure and distribution patterns are determined by organic matter type and origin, which is further investigated in the paper.

4.2. Major and Trace Element Composition, Sm and Nd Isotopes

The elemental composition was determined for 131 samples taken at regular intervals along the section (the average distance between the samples is 15–25 cm) using portable XRF. In the resulting data set (Tables A1 and A2), significant variations in the elemental composition relative to the average values for the Abalak and Bazhenov Formations were identified. Therefore, we specified geochemical levels within the section.

Considering the characteristic paleo-geographic features of black shale formations [30,38], we paid special attention to the lithological composition and genesis of rocks: fluctuations in redox conditions, changes in the input of terrigenous and biogenic material, and bioproductivity of the paleo-sea.

According to the methods described in [39–41], we have calculated a set of lithochemical proxies, which were used to identify the genesis of rocks (Figure 4). The most informative components to assess the contribution of terrigenous clastic components are Al, Ti, Zr, K, and the authigenic and biogenic components of the rock: S, P, Mo, Ca, Mg, Ni, Cu, Zn, V, etc. [41,42]. The carbonate content was studied via the ratios of Ca, Mg, Sr, Mn, and Fe. The predominant type of iron minerals (oxide, sulfide forms, the Fe affinity with S, Mn, and Ni) was revealed. Some of the proxies allowed us to assess paleo-facial conditions: dissolved oxygen concentration, depth fluctuations, distance to the source of terrigenous flux.

The total terrigenous contribution was estimated by the parameter (Al + K)/(Si + Ca + Mg), which was chosen specifically for siliceous black shales [30]. Unchanged ratios of chemical elements of terrigenous origin (Al, K) indicate the stable composition of the incoming terrigenous suspension. Mg is the main component of many clays, and Si can be of different origin: terrigenous (quartz grains, alumosilicates), biogenic (radiolarians), secondary (silicification). Variations in Ti/Zr, Ti/Al, Mg/Al, K/Al, and Rb/K are associated with the evolution of the terrigenous source or the contribution of several sources [40,41]. According to the increase in Zr (we consider the Ti/Zr ratio), one can reconstruct the distance to the terrigenous source, since Zr is the most stable component in the geochemical environment [40]. The absence of correlations between the contents of Si, Mg, and Fe and Al, Zr, Ti, and K, as well as a disproportionate excess of (Si + Mg + Fe) relative to (Al + Zr + Ti + K), indicates their authigenic origin and biogenic source.

The considered rocks contain a low amount of carbonate minerals, and the absolute carbonate content was determined for individual samples only (see Section 4.6). Relative carbonate content variations were evaluated by the ratio (Ca + Mg)/(Al + Si), where Ca and Mg are from the carbonate fraction, and Al and Si are attributed to the siliciclastic fraction and have terrigenous and mixed terrigenous-biogenic origin, respectively. Qualitative changes in the carbonate composition are caused by the source of carbonate matter (Sr/Ca [39]), depth and oxygen concentration (Mn/Ca), and partly by the total Mg content of the rocks (Mg/Al).

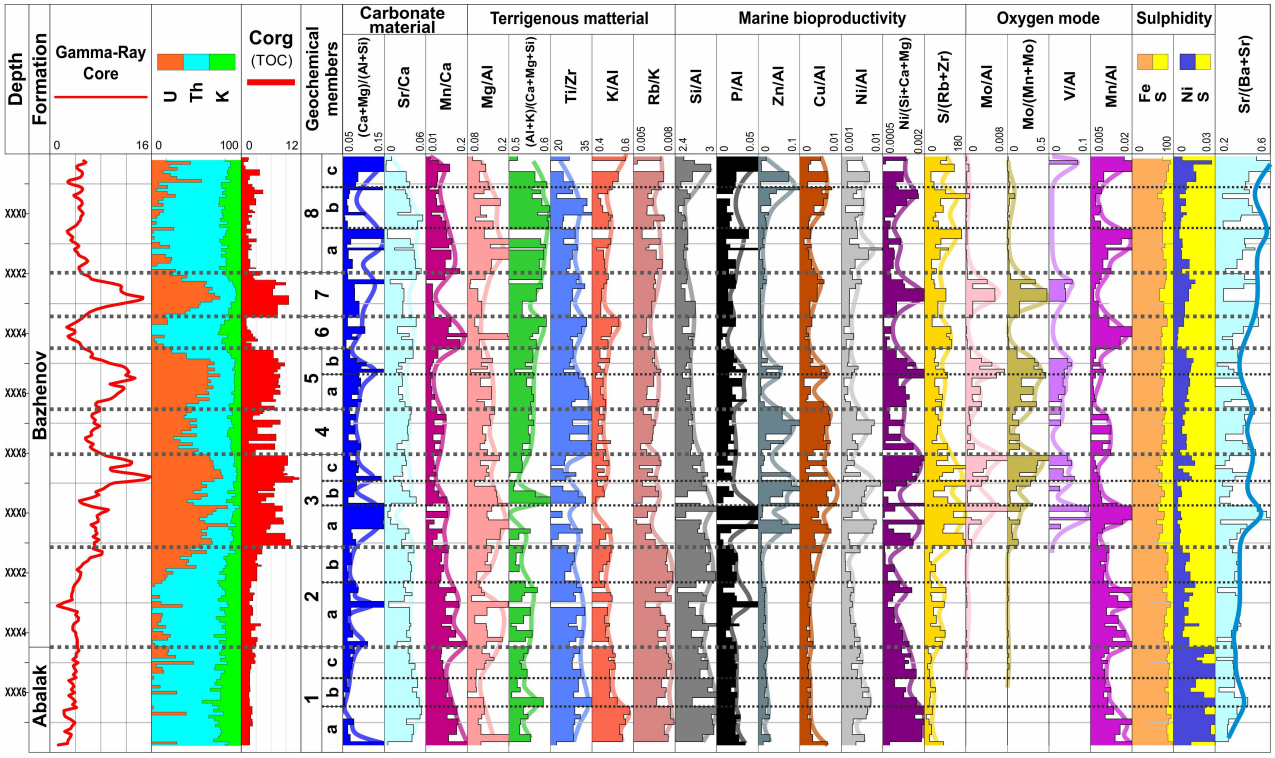


Figure 4. Geochemical structure of the section and variability of the values for geochemical members.

The contents of the most significant biophilic elements normalized to Al and some terrigenous elements were used as indicators of paleo-bioproductivity: P/Al, Si/Al, Mo/Al, S/(Rb + Zr), Zn/Al, Cu/Al, and Ni/Al. The amount of P and S in sedimentary rocks is predominantly controlled by biogenic material. Integration of the proxies is necessary, since the redox conditions were not stable during the accumulation of the studied deposits.

Water chemistry and element influx into a basin associated with terrigenous sediments can also impact the enrichment pattern of redox-sensitive trace elements. This controls the applicability of trace element-based redox proxies. In general, Mo, V, Ni, Cu, and Zn concentrate into the sediment under oxygen-depleted and anoxic environments together with organic matter [38,39,41,43,44]. The most sensitive indicators of the oxygen level for the rocks of the Bazhenov Formation are the ratios Mo/(Mn + Mo), V/Al, and Mn/Al [38–41]. Mn mainly exists in oxide mineral form, and therefore is not typical for sediments accumulated in anoxic conditions. Mn is one of the most sensitive indicators of oxygen concentration, and thus we consider the ratio Mn/Al.

The sulfur and sulfide content in the section is determined by several parameters: bioproductivity, anoxic conditions, and sedimentation rate. The sulphidity in the section is analyzed using the ratios of S and Fe, as well as S and Ni. In anoxic conditions, Fe and redox-sensitive metals exist mainly in the form of sulfide [38–41]. The total content of authigenic sulfur and its predominance over the terrigenous fraction was estimated by the S/(Rb + Zr) ratio, in which characteristic trace elements were used as a terrigenous indicator. Ni in rocks allows us to assess the authigenic biogenic contribution (by the direct relationship of Ni with S and other biophilic elements) or to reveal the introduced components (positive correlations of Ni with Fe, Mn, and terrigenous components).

One of the possible indicators of eustatic fluctuations with the relative stability of the drift sources is the ratio of Sr and Ba. The behavior of these elements in the marine geochemical environment is different, and the Sr content increases with increasing distance from the watershed (Sr/(Ba + Sr) ratio increases) [40,41], while Ba-based proxies should be used with caution in case of the alteration of redox conditions.

During analysis of the elemental proxies, the frequent changes in rock composition along the interval were detected, and the section could be subdivided into 16 geochemical

levels (Figure 4). We combined the levels into eight geochemical members based on the data on gamma-spectral core profiling (U, Th, K), lithology, and TOC (Figure 4, Table 1); members were considered to study rather general trends in paleoenvironment changes rather than the individual events.

Table 1. Geochemical members and their distinctive characteristics: TOC (pyrolysis) and U content according to gamma-ray spectrometry, genesis type.

Member	TOC, wt.%	U, ppm	Lithotype	Sedimentation Type	Sedimentation Conditions
#8	0.47–4.35 [1] 2.00 [2]	0–17.33 2.7	L-4	Terrigenous with periodical mixed terrigenous and biogenic	Enhanced terrigenous influx with increased bioproductivity events
#7	6.35–9.57 7.60	8.8–39.8 23.4	L-3	Mixed terrigenous and biogenic	Predominantly anoxic conditions, sea level transgression
#6	0.95–3.31 1.93	0.0–3.7 1.8	L-4	Terrigenous	Hydrodynamic activation of bottom waters, the presence of oxygen, enhanced terrigenous influx
#5	4.00–8.74 7.13	6.0–30.9 20.8	L-3	Mixed terrigenous and biogenic	Predominantly anoxic conditions, sea level transgression
#4	1.48–7.83 4.30	4.9–16.1 10.6	L-2	Mixed terrigenous and biogenic	The first episode of a new source of terrigenous influx, weak terrigenous inflow, suboxic environment
#3	5.06–11.62 7.79	6.0–44.1 19.6	L-3	Mixed terrigenous and biogenic	Predominantly euxinic conditions, sea level transgression
#2	1.63–4.33 2.80	0.0–10.9 2.5	L-1	Transitional from terrigenous to mixed terrigenous and biogenic	Start of sea level rise, transition from terrigenous to biogenic sedimentation
#1	1.55–3.26 2.16	0.0–8.0 1.1	L-1	Terrigenous	Shallow sea with the presence of oxygen and moderate terrigenous inflow

[1] Range of values. [2] Average value.

Member #1 (3.5 m) is subdivided into three geochemical levels (1a, 1b, 1c), and the interval corresponds to the upper part of the Abalak Formation and is characterized by relatively high contents of terrigenous Fe, Ni, and Mn, low carbonate content, low contents of S and pyrite, and low concentrations of biophilic elements (Mo, V, and other transition metals), which refer to the presence of oxygen during sedimentation. Geochemical level 1a is characterized by the highest contents of non-biogenic Ni and Mn, by high K/Al, and by low Sr/Ba ratio. The sedimentation conditions of these rocks correspond to a shallow and well-aerated sea basin with a moderate terrigenous input, which is consistent with previously reported data [26,27]. For the above laying levels 1b and 1c, we observe slight fluctuations in sea level detected by Sr/(Ba + Sr), clay content (Al + K)/(Ca + Mg + Si), Ti/Zr, and a stepwise decrease in Ni concentrations as Ni/S and Ni/(Si + Ca + Mg) and Mn as Mn/Al and Mn/Ca.

Geochemical member #2 (3 m) corresponds to the beginning of sedimentation of the Bazhenov Formation, which was established by the simultaneous prompt increase in the content of sulfur and sulfides, organic carbon, and Mo. Its lower level (2a) corresponds to a hydrologically active facies, which follows from the abrupt increase in Mn and P as well as fluctuations in clay content. The upper level (2b) has lower Mn, increased biogenic silica (Si/Al), and a decreased clay content, which can be associated with a slow rise in the sea level, as estimated from an increase in Sr/(Ba+Sr).

The bottom of geochemical member #3 (3 m) is the most distinct level in the section, characterized by the growth of biophilic S, Mo, Ni, Cu, Zn, changes in the concentrations of P, Ca, Sr, and Mn, with the lowest clay content within the section. The observed changes are in good agreement with the increase in U, S, content, total radioactivity, and TOC. Here, we interpret a rapid rise in sea level, which led to the weakening of the existing sources of terrigenous flux and subsequently to the change in the sedimentation to the biogenic regime. The transgressive period is marked near the boundary of levels 3a and 3b by the excess of P and Mn and minimum content of terrigenous components (Al, K, Ti, Zr), which all together indicates an active hydrological regime. Geochemical level 3b is distinguished by a short-term increase in clay content and a high content of redox-sensitive metals. Level 3c is characterized by the appearance of a stable anoxic environment with the accumulation of abnormally high organic matter content and the associated concentration of biophilic metals (Mo, V, Ni, U).

Rocks of member #4 (1.5 m) have an increased content of terrigenous material and decreased organic matter content, which coincides with lower gamma values and must result from moderate or periodical exposure to oxygen. The Ti/Zr, K/Al, and Si/Al ratios demonstrate a different composition of terrigenous material supplied to the area of sedimentation with respect to lower members #1 and #2. From this depth, biogenic silica accumulation is inhibited by the increasing volumes of clay. Member #4 is interpreted as an episode of the appearance of a new source of terrigenous material, the influence of which will gradually increase until member #8.

The composition of rocks from member #5 (2 m) reflects an episode of anoxia with intensive biogenic sedimentation, resulting in the accumulation of a large amount of TOC. Increased Mo/Al, Mo/(Mo + Mn), V/Al maximum and low Mn/Al ratios indicate that the anoxic environment expands from the bottom to the upper part of the member. The event of elevated bioproductivity is characterized by an increase in (Ca + Mg)/(Al + Si), P/Al, Cu/Al, Ni/(Si + Ca + Mg), Mo/Al, and Mo/(Mo+Mn), with a simultaneous decrease in terrigenous components (Ti/Zr, Mg/Al and others), and marks the boundary between two geochemical levels in member #5: the upper one (5b) corresponds to a more pronounced period of euxinia and organic matter accumulation, as it follows from TOC content, Mo and Ni proxies. The composition of terrigenous material is stable, according to qualitative proxies (K/Al, Rb/K, Si/Al, (Al + K))/(Ca + Mg + Si).

In member #6 (1 m), an intensive terrigenous inflow and reduced amounts of organic matter in the sediment are reconstructed by an increase in (Al + K)/(Ca + Mg + Si), Ti/Zr, and K/Al ratios. Such sedimentation conditions are associated with hydrodynamic activation of bottom currents and water aeration, which can be derived from increased Mn/Ca, Mn/Al ratios. The resulting accumulation of organic matter is reduced both by oxidative degradation of organic matter and dilution by significant amounts of clay material.

Member #7 (1 m) is the next stage of marine bioproductivity, with a reduced role of terrigenous sedimentation. An enriched in TOC member #7 was formed under a stable deep anoxic environment and anomalous enrichment in redox-sensitive Ni, V, and Mo was detected (the maxima for U, Mo/Al, Mo/(Mo + Mn), V/Al, Ni/(Si + Ca + Mg) and elevated Cu/Al are found). At the same time, terrigenous influx is moderate and its composition is stable, as it follows from (Al + K)/(Ca + Mg + Si), K/Al, and Ti/Zr. A thin carbonate layer is present in the upper part of the member, formed during the transition to oxic conditions (refer to Mn/Al), resulting in the drop in TOC accumulation at the boundary of members #7 and #8.

Member #8 (5 m) shows the most significant variations of composition and exhibits fluctuating enrichment in terrigenous components, with an occasional occurrence of biophilic components and organic matter in the rocks. It could be subdivided into three geochemical levels (8a, 8b, 8c). The depositional environments for 8a and 8c are close to that of member #6, with oxic conditions and intensive terrigenous influx, whereas for 8b, a suboxic environment is assumed. The rocks of 8b show increased clay content (Al + K)/(Ca + Mg + Si), and Ti/Zr; in 8c, P, Ca, K/Al and Si/Al are increased. In general, member

#8 is the less stable one in terms of sedimentation conditions, while the predominant regime is terrigenous sedimentation with low degree TOC accumulation.

Thus, lithological and geochemical data of the studied section indicate the homogeneity of the upper part of the Abalak deposits (member #1), transition to mixed terrigenous and marine sedimentation in #2 and #3 and alternation of the members with different genesis in the upper members #3-#8 (Figure 4, Table 1). This alternation is caused by periodically increasing terrigenous influx and water oxygenation (members #4, #6, #8), and in between the sedimentation conditions were favorable for the concentration and preservation of organic matter (#3, #5, and #7) due to a low sedimentation rate, a high proportion of the biogenic component, and predominantly anoxic conditions. Several parameters indicate that the studied marine basin gradually expanded and deepened. An increase in the volume and depth of the basin started during member #2 accumulation led to the decreasing hydrodynamic activity of the bottom layers, which contributed to a gradual increase in the proportion of clay sedimentation (from member #4 to #8).

For 14 samples from the members accumulated under different sedimentation conditions, we used TIMS method to measure the content of Sm, Nd and isotope ratios $^{147}Sm/^{144}Nd$, $^{143}Nd/^{144}Nd$ (Table 2, Figure 5). Variations in the isotopic composition of Nd along the section indicate the existence of at least two different terrigenous sources and their variable role in sedimentation.

Table 2. Sm and Nd content and isotope composition (TIMS), $(^{143}Nd/^{144}Nd)_i$ is the ratio corrected for the time of the Bazhenov Formation sedimentation.

Member #	Sm	Nd	$^{147}Sm/^{144}Nd$	$^{143}Nd/^{144}Nd$	$(^{143}Nd/^{144}Nd)_i$
units	ppm	ppm			
8	1.53	7.47	0.1242	0.512267	0.512149
8	6.49	32.54	0.1205	0.512266	0.512152
8	6.99	37.32	0.1132	0.512258	0.512150
8	4.37	24.58	0.1075	0.512279	0.512177
8	2.98	18.67	0.0967	0.512248	0.512156
7	6.45	29.84	0.1307	0.512250	0.512125
7	5.95	27.30	0.1318	0.512247	0.512122
7	6.15	28.90	0.1286	0.512252	0.512130
7	6.61	30.98	0.1289	0.512233	0.512110
6	3.50	22.74	0.0932	0.512259	0.512170
5	7.09	32.59	0.1315	0.512209	0.512084
4	10.81	53.75	0.1216	0.512212	0.512096
3	7.48	32.17	0.1405	0.512223	0.512090
1	5.45	28.00	0.1177	0.512264	0.512152

There are members characterized by mixed terrigenous and biogenic sedimentation #3, #4, #5, and #7, and their characteristic $^{143}Nd/^{144}Nd$ values do not exceed 0.512130 (Figure 5). The increase in Nd isotope ratio for the members #1, #6, and #8 reflects an increase in terrigenous influx from the sources with higher values of $^{143}Nd/^{144}Nd$: 0.512152, 0.512170, and 0.512149-0.512177, respectively.

According to [45,46], the material in the modern estuarine sediments of the Ob River (weathering crust of the Urals) has a lower isotopic ratio of Nd as compared to the Yenisei river deposits (weathering crust of the Siberian platform). The $^{143}Nd/^{144}Nd$ values for the estuarine sediments of the Yenisei River are 0.512132–0.512167 (corrected for the time of the Bazhenov Formation sedimentation), which correlates with the measured values for members #1, #6, and #8 in the studied section (Figure 5). For the estuarine sediments of the Ob River, the values are in the range 0.512101–0.512139 (corrected for the time of the Bazhenov Formation sedimentation), which overlap with the $^{143}Nd/^{144}Nd$ values for the samples from member #7.

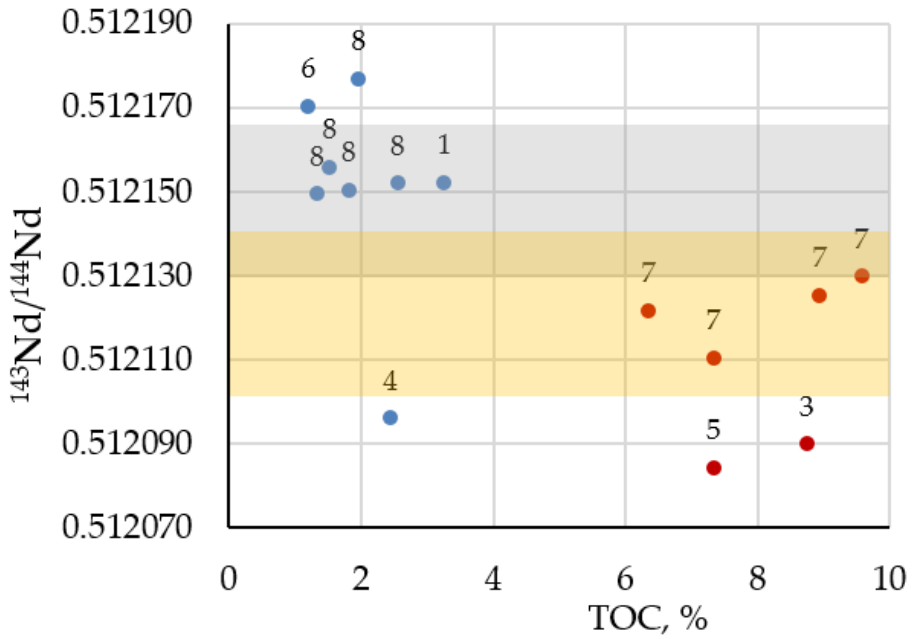
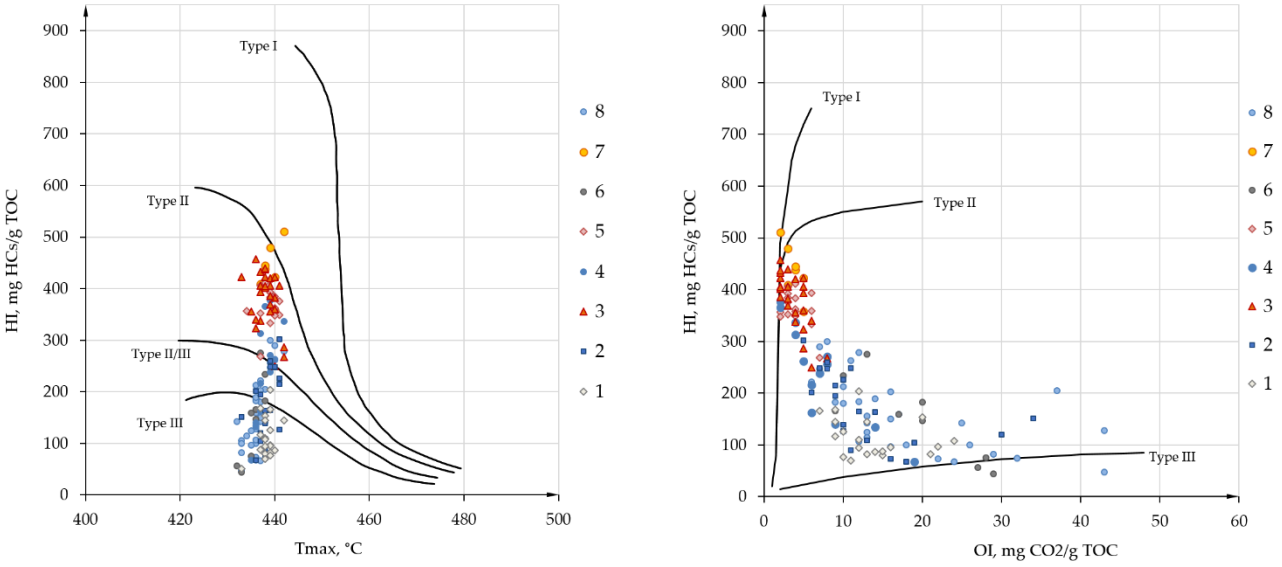


Figure 5. Nd isotope ratio vs. TOC plot. The characteristic values of $^{143}Nd/^{144}Nd$ ratios are given by shaded areas for weathering crust of Siberian Craton (grey) and Urals (yellow) (corrected for the time of the Bazhenov Formation sedimentation).

4.3. Source Rock Characterization

We performed source rock characterization and TOC measurements for 150 samples within the studied section. The results are shown in Figures 6 and 7 and Table A3.



(**a**) (**b**)

Figure 6. (**a**,**b**) Modified van Krevelen plots for the samples from the studied section. Red and orange markers are used for members #3, #5, and #7 (average TOC > 5 wt.%), grey and blue are for members #1, #2, #4, #6, and #8 (average TOC < 5 wt.%).

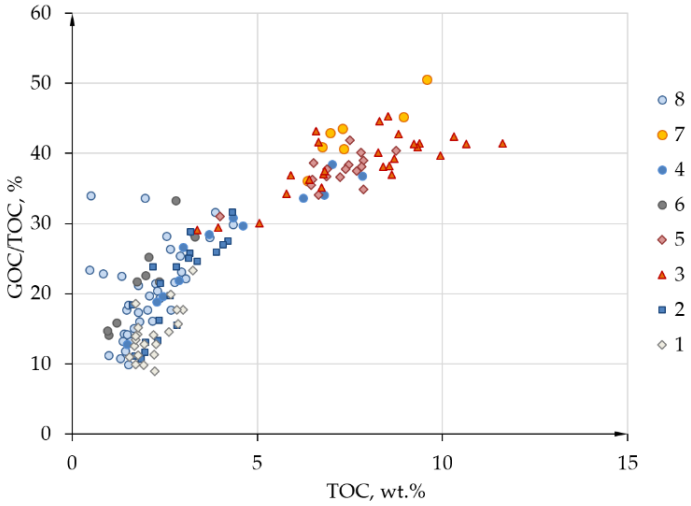


Figure 7. Cross-plot of TOC and generative organic carbon (GOC/TOC, %) for the samples from the studied section. Red and orange markers are used for the members #3, #5, and #7 (average TOC > 5 wt.%), grey and blue are for the members #1, #2, #4, # 6, and #8 (average TOC < 5 wt.%).

According to the average TOC values for eight geochemical members (Tables 1 and A3), intervals with TOC < 5 wt.% can be considered as being depleted of organic matter to different extents (members #1, # 2, # 4, #6, and #8), and three members with TOC > 5 wt.% (#3, #5, and #7) are enriched in TOC, although individual samples within each member can show higher or lower organic matter content (Figure 7).

The maturity of the organic matter in the studied section corresponds to the beginning of the oil window. The values of Tmax vary between 434 and 442 °C, with an average of 438 °C (Figure 6a).

The members with the increased role of biogenic sedimentation, member #3, #5, and #7, are enriched in TOC, and the rocks contain type II kerogen. They are potential oil source rocks. The hydrogen index HI varies from 249 to 511 mg HC/g TOC, and OI is below 6 mg CO_2/g TOC with the only one exception (Figure 6b).

The organic matter from members #1, #2, #4, #6, #8 are mixed type II/III kerogen, with HI varying in a range from 44 to 300 mg HC/g TOC with a few exceptions, and moderate OI is from 5 to 30 mg CO_2/g TOC for most of the samples. The significant admixture of humic organic matter with higher OI and lower HI is observed for the rocks in members #1, #2, #6, #8, whereas the individual samples from #4 contain type II kerogen.

These results are further confirmed by analysis of the composition and kinetics of kerogen thermal decomposition products.

The share of pyrolyzable carbon in TOC (GOC/TOC, %) is 10–30% for the samples from members #1, #2, #4, # 6, and #8 and 35-45% for the rocks from TOC-enriched #3, #5, and #7 with type II kerogen, with minor exceptions (Figure 7). Differences in GOC/TOC with the same thermal history and maturity within the studied 20 m originate from the composition of the initial organic matter and the differences in the kinetic characteristics of kerogen transformation to hydrocarbons.

4.4. Kerogen Thermal Decomposition Kinetics and Products

Analysis of kerogen decomposition products and bulk kinetics studies were used to obtain additional data on kerogen type, maturity, and petroleum generation characteristics for each member in accordance with the depositional environment.

The TOC-enriched intervals contain organic matter with the same kinetic characteristics (Figures A1 and A2). Approximately 50% of the matter undergoes decomposition at 52 kcal/mol, 40% at 53 kcal/mol, and the remaining 10% at 55–56 kcal/mol. The decomposition spectra of kerogen in the intervals depleted in TOC (#1, #2, #4, #6, and #8) varies and depends on marine and terrestrial organic matter proportion (Figure A1). The obtained

activation energy distributions allow one to estimate the degree of kerogen transformation into hydrocarbons for the chosen conditions: for the samples #1, #2, #3, #5, #7, and #8, it is about 90–95%, and for intervals #4 and #6, it equals 80%, indicating differences in kerogen composition.

Using flame ionization detector (FID) response in pyro-GC analysis, we calculated the distribution of different classes of compounds: gas and low-boiling liquid hydrocarbons (C1–C7), aliphatic (alkanes, cycloalkanes, and unsaturates), and aromatic components (mono-, di-, tricyclic) (Table 3).

Table 3. Kerogen cracking products distribution obtained at 500°C and 0.5 min exposure time, calculated in % of total FID response.

Member #	Gas and Light HCs, %	Aliphatic Compounds, %		Aromatic Compounds, %			Aliphatic/ Aromatic Ratio
		Alkanes	Unsaturates, Cycloalkanes	Mono-Aromatics	Di-Aromatics	Tri-Aromatics	
8	44	6	0	37	11	2	11/89
7	7	7	24	19	14	29	33/67
6	20	6	4	31	25	14	13/87
5	8	5	21	19	21	25	29/71
4	20	7	6	33	23	11	16/84
3	11	10	30	16	13	20	45/55
2	16	17	16	19	12	20	39/61
1	36	9	2	35	16	3	17/83

Rock samples collected from intervals #1 and #8 contain gas-prone kerogen, which generates 36 and 44% percent of gas at elevated temperature, respectively. The aliphatic/aromatic compounds ratio is useful for oil hydrocarbons characterization since it correlates with oil density and viscosity. For intervals #1 and #8, the ratio is 17/83 and 11/89, respectively. Kerogen in rocks enriched with TOC (members #3, #5, and #7) is oil-prone, giving less than 10% of gas and oil with an aliphatic/aromatic ratio higher than 30/70. Intervals #2, #4, and #6 are in between two distinctive groups. There is 20% of gas in pyrolysis products for #4 and #6, and the aliphatic/aromatic ratio is around 15/85, whereas for #2, the composition is close to oil-prone intervals: the gas share is 16% and the aliphatic/aromatic ratio is 39/61. Therefore, kerogen in #2, #4, and #6 is classified as mixed oil- and gas-prone.

4.5. Thermal Extraction and Biomarker Analysis

Based on source rock characterization and analyses of kerogen decomposition products, nine samples were selected for biomarker analysis. These samples roughly represent common characteristics of organic matter and mobile hydrocarbon composition for each member, although the variations of composition within each interval are more significant. Since thermal extraction TD-GC×GC-MS (at 350 °C) is an express alternative to organic solvent extraction [47,48], we applied this approach for the analysis. The results are presented in Figures 8 and 9, and in Table 4.

The intervals enriched in TOC #3, #5, and #7 contain hydrocarbons similar to rock extracts and oils from the Bazhenov core in the central part of the West Siberian Basin, which were formed in deep-sea anoxic conditions from marine organic matter [9,49,50]. The main components of the extracts are petroleum hydrocarbons with a proportion of aliphatic components of about 80%, and that of aromatic components of no more than 10%. The maximum of the *n*-alkanes distribution corresponds to *n*-C_{11}-C_{13} (Figure 8). The extracts are characterized by molecular parameters and biomarkers of marine organic matter accumulated in suboxic conditions: Pr/Ph is in the range 2.3–2.6, the full distribution of homohopanes C31-C35, high C35 homohopane index, Ts/Tm = 0.9–1.5, C29/C30Hop = 0.5–0.7, the predominance of C27 in the distribution of regular steranes [20–22,51] and the samples are attributed to the area of mixed origin oils at the plot considered in [50] for the Bazhenov oils (Figure 9b). The regular steranes distribution is the only parameter that indicates the increasing terrigenous organic matter input in TOC of members #2, #3, #5,

and #7: the share of C29 increases from #2 and #3 to #5 and #7 (19,19,21,26%, respectively) with the simultaneous decrease in C27.

The extracts from the depleted-in-TOC intervals #1, #2, #4, #6, and #8 differ from each other due to different depositional environments, and below we discuss the key features for each of the members.

Hydrocarbons in the rock from member #1 are condensate that contain alkanes, mono- and di-aromatic components. The distribution of *n*-alkanes is narrow, with a pronounced maximum at *n*-C_{15}. The extract contains no hopanes, steranes, or triaromatic steroids (TAS_), which is the evidence for oxic depositional environment and humic organic matter input [51].

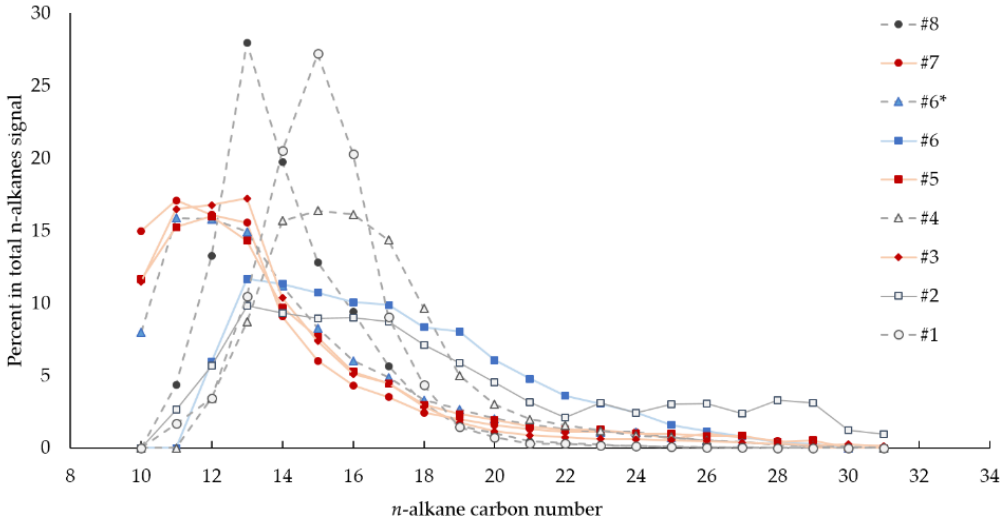


Figure 8. *n*-Alkanes distribution for thermal extracts of the rocks from the members #1 to #8 (thermal extraction at 350 °C).

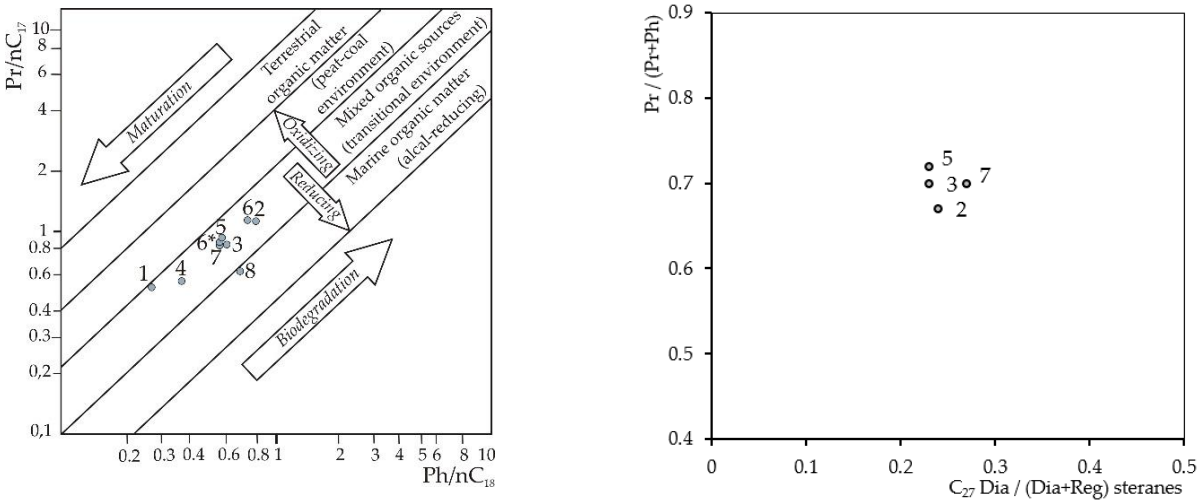


Figure 9. Pr/*n*-C17 ratio vs. Ph/*n*-C18 ratio (**a**) and pristane/(pristane+phytane) ratio vs. C_{27} steranes Dia/(Dia+Reg) ratio (**b**) for thermal extracts of the rocks from the members #1 to #8 (thermal extraction at 350 °C).

Table 4. Selected molecular and biomarker parameters of thermal extracts.

Parameter [1]	Member #								
	1	**2**	**3**	**4**	**5**	**6***	**6**	**7**	**8**
Pr/Ph	4.20	2.07	2.38	3.03	2.53	2.39	1.88	2.34	1.90
Pr/(Pr + Ph)	0.81	0.67	0.70	0.75	0.72	0.71	0.65	0.70	0.65
Pr/*n*-C17	0.53	1.13	0.87	0.57	0.94	0.88	1.15	0.87	0.68
Ph/*n*-C18	0.26	0.79	0.58	0.36	0.55	0.54	0.73	0.54	0.67
Ki	0.44	0.97	0.76	0.49	0.78	0.74	0.96	0.74	0.67
n-C27/*n*-C17	0.00	0.70	0.08	0.02	0.19	0.08	0.08	0.20	0.01
MNR	0.79	0.63	0.99	0.87	0.85	0.74	0.58	0.91	0.84
4/1-MDBT	2.33	2.08	2.39	2.43	2.13	3.52	2.75	2.23	2.33
MPI	0.41	0.38	0.50	0.29	0.26	0.33	0.54	0.38	0.59
TAS	none	0.41	0.53	0.99	0.52	n/a	n/a	0.49	none
Aliph/Arom	9.2	24.5	7.4	7.3	13.1	21.8	7.4	8.4	7.1
Dia/(Dia + Reg) C_{27} steranes	none	0.24	0.23	traces	0.23	traces	traces	0.27	traces
Regular steranes, %									
C27	none	55	58	traces	48	traces	traces	46	none
C28	none	27	23	traces	30	traces	traces	29	none
C29	none	19	19	traces	21	traces	traces	26	none
Terpanes									
Ts/Tm	none	0.94	1.51	0.98	1.51	3.11	1.95	1.23	traces
C29/C30Hop	none	0.53	0.74	1.16	0.61	0.96	1.46	0.61	1.06
C31H	none	0.69	0.60	traces	0.60	traces	traces	0.64	none
Homohopanes distribution, %									
C31		49	46		50			50	
C32		32	36		36			34	
C33	none	27	27	traces	26	traces	traces	25	traces
C34		18	20		19			18	
C35		14	16		14			14	

[1] Pr—pristane, Ph—phytane, *n*-C_X—linear alkanes with X carbon atoms, Ki—(Pr + Ph)/(*n*-C_{17}+*n*-C_{18}) (*m*/*z* 57), MNR—2- to 1-methylnaphthalene ratio (*m*/*z*. 142), 4/1-MDBT—4- to 1-methyl-dibenzothiophene ratio (*m*/*z*. 198), MPI—(9+1)- to (2+3)-methyl-phenanthrene ratio (*m*/*z*. 192), TAS—short- to long-chain triaromatic steroids (*m*/*z*. 231), Aliph/Arom—aliphatic (alkanes, cycloalkanes, unsaturates) to aromatic (mono-, di-, tri-) compounds ratio (FID); terpanes: Ts—18a(H)-22,29,30-trisnorneohopane, Tm—17a(H)-22,29,30-trisnorhopane, Ts/Tm—trisnorhopane ratio (*m*/*z*. 191).

The extract from member #2 combines features of both marine and terrigenous organics. *n*-alkanes distribution is wide, and there is an elevated concentration of long-chain alkanes from *n*-C_{22} to C_{30}. At the same time, the composition of sterane and hopane biomarkers is close to that of #3, which is the result of the transition from terrigenous in #1 to marine sedimentation that took place during member #3 accumulation.

For the studied deposits starting from member #3, accumulation of predominantly marine sapropelic organic matter in anoxic conditions periodically was interrupted by terrigenous material influx and water oxygenation which resulted in the dilution of organic matter by siliclastic material, the significant increase in sedimentation rate and lower degree of organic matter preservation.

The extractable organic matter in the sample from member #4 is represented by alkanes, mono- and di-aromatic components. The distribution of *n*-alkanes is broadened, and the maximum corresponds to *n*-C_{13}-C_{16}. The terpane ratios are Ts/Tm = 1, C29/C30Hop = 1.2. A distinctive feature of the extract is the presence of short C20 and C21 triaromatic steroids without higher homologs, TAS = 1. All parameters indicate that organic matter has a predominantly marine genesis, with a significant admixture of terrigenous as compared to members #3, #5, and #7.

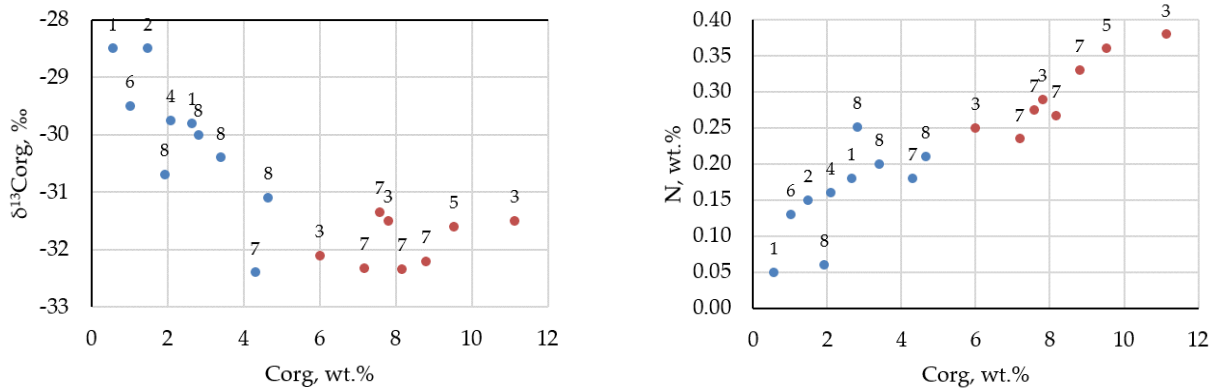
Member #6 is an interval with easily recognizable lenses with different TOC. We performed two analyses of the extracts: for lighter and darker colored rocks. In the dark-

colored sample, the distribution of *n*-alkanes is identical to that of the intervals #5 and #7 with high TOC (Table 4, Figure 8, see sample 6*). At the same time, in the lighter colored rock (sample 6), the distribution is wide, in a range from *n*-C12 to C20, without a pronounced maximum. There are no steranes and TAS. The terpane ratios are Ts/Tm = 2–3, C29/C30Hop = 1.0–1.5. Member #8 is a heterogeneous interval. For the selected sample, the ratio Ts/Tm = 0.8, C29/C30Hop = 1.1.

The extract composition for the members with TOC < 5 wt.% is determined by the admixture of terrigenous organic matter and oxidative accumulation conditions. Regular steranes composition indicates the increasing influx of terrigenous organic during predominant biogenic sedimentation: the admixture increases from #2 and #3 to #5 and #7.

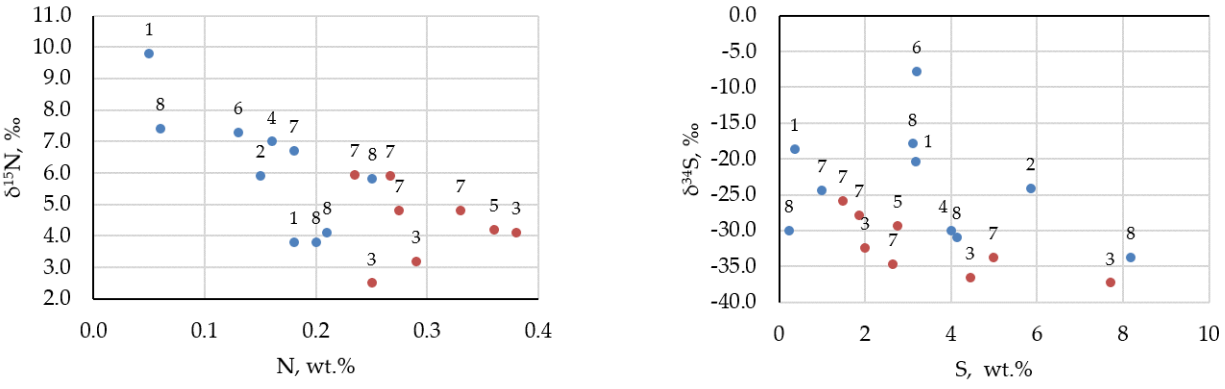
4.6. Elemental and Isotope Composition of Carbon, Nitrogen, and Sulfur

The isotopic composition and content of organic carbon, nitrogen, sulfur and carbonate carbon, and oxygen were determined in 18 selected samples from all members (Figures 10 and 11 and Table A4).



(**a**) (**b**)

Figure 10. (**a**) Cross-plot of the elemental and isotopic composition of organic carbon. (**b**) Cross-plot of the elemental composition of nitrogen and organic carbon. The two series of samples represent rocks with C_{org} < 5 wt.% (blue markers) and C_{org} > 5 wt.% (red markers), and numbers correspond to geochemical members.



(**a**) (**b**)

Figure 11. (**a**) Cross-plot of the elemental and isotopic composition of nitrogen. (**b**) Cross-plot of the elemental and isotopic composition of sulfur. The two series of samples represent rocks with C_{org} < 5 wt.% (blue markers) and C_{org} > 5 wt.% (red markers), numbers correspond to geochemical members.

The organic carbon concentrations measured using elemental analyzer (C_{org}) are consistent with the TOC values obtained by pyrolysis and vary from 0.5 to 11.1 wt.%. The isotopic composition of organic carbon takes the range of $\delta^{13}C_{org}$ from −32.4 to −28.5‰ (PDB) (Figure 10a). Samples with an organic carbon content higher than 5% are depleted in ^{13}C with $\delta^{13}C_{org}$ from −31.3 to −32.4‰, as compared to samples with organic carbon content below 5 wt.% with $\delta^{13}C_{org}$ in the range from −31.1 to −28.5‰.

The difference in isotope composition correlates with the difference in the environment of organic matter accumulation and its origin, which results in high and low TOC. According to [2,52], for the Bazhenov Formation, the $\delta^{13}C_{org}$ below −30‰ is characteristic for the marine polymer-lipid type of organic matter (#3, #5, and #7), while higher and more positive values reflect the input of organic matter of terrigenous origin, as in #1, #2, #4, #6, and #8.

The concentrations of nitrogen in the investigated samples vary from 0.05 to 0.38 wt.% and demonstrate a strong positive correlation with organic carbon concentrations, indicating the organic source of nitrogen (Figure 10b). The $\delta^{15}N$ is in the range from 2.5 to 9.8‰ (AIR) (Figure 11a), and samples with C_{org} > 5% are depleted in ^{15}N, with $\delta^{15}N$ values from 2.5 to 5.9‰; meanwhile, samples with low C_{org} are generally enriched in ^{15}N, and the $\delta^{15}N$ value range is from 3.8 to 9.8‰ and tend to increase with decreasing organic carbon concentration. Observed C/N ratios are affected by both organic matter source and diagenetic alterations, and for high-TOC members, C/N varies in a narrow range, 24–31, whereas samples from low-TOC members show lower ratios, 8–22, that decrease with decreasing C_{org}. The only exception is the sample with C/N 32, which has C_{org} 0.6 wt.% and C_{carb} 9.9 wt.%. These variations also speak in favor of the presence of organic matter of different origin in layers with high and low TOC.

Total sulfur content in the investigated rocks takes a wide range of values from 0.2 to 8.2 wt.%, exhibits a positive correlation with iron content, and no correlation with organic carbon concentration (Figure 11b). The main chemical form of sulfur is sulfide sulfur fixed as pyrite. Organic sulfur is present in a subordinate amount, since its content in organic matter in sedimentary rocks of the Bazhenov Formation is generally low and does not exceed 5 wt.% [2]. In contrast to sulfur concentration, the isotopic composition of sulfur demonstrates correlation with organic carbon concentration, the $\delta^{34}S$ values from −33.7 to −7.8‰ are significantly higher for the samples with TOC < 5 wt.% than for the samples enriched in TOC with the $\delta^{34}S$ from −37.3 to −25.8‰ (Figure 11b). The isotopic composition of sulfide (S^{2-}) in sediments is controlled by the degree of bacterial reduction of sulfate ($SO4^{2-}$) dissolved in water since the produced H_2S is then used for pyrite formation and organic matter sulfurization. The process is affected by the redox environment in the bottom water layer and sediment column [53]. Under suboxic to euxinic conditions, sulfate reduction occurs both in bottom water and upper sediment layers (beneath the water–sediment interface). The system is open with respect to sulfate, and even at high sulfate reduction rates, the hydrogen sulfide and formed pyrite express very negative $\delta^{34}S$ values due to the kinetic isotope effect between $SO4^{2-}$ and H_2S, which can reach −66‰ [54]. Under oxic conditions, there is no sulfate reduction in water and upper sediment layers. It only takes place in pore water of deeper buried sediments. Thus, the system is closed with respect to sulfate, and in the case of sulfate exhaustion, the hydrogen sulfide and pyrite can reach positive $\delta^{34}S$ values. According to these mechanisms, low $\delta^{34}S$ values and high organic carbon content in the investigated samples reflect suboxic to euxinic conditions in the paleo-sea, low organic carbon content (#3, #4, #5, #7, and #8) and higher $\delta^{34}S$ values corresponding to oxic conditions during sedimentation (#1, #2, and #6).

The carbonate carbon content is generally low in the studied sedimentary sequence, and C_{carb} is less than 1 wt.% for most of the samples. Only three layers in investigated section demonstrate higher carbonate contents: one layer in the lower part (#1, sideritized argillaceous-siliceous rock) and two in the upper part (#7 and #8, calcified radiolarite), with C_{carb} 8.1, 5.1, and 9.9 wt.%, respectively (Table A4). Samples from the middle part of the

section (members #2–7) are weakly carbonated siliceous-argillaceous, argillaceous-siliceous and argillaceous rocks.

The carbonate carbon and oxygen isotopic composition vary considerably within the studied section: $\delta^{18}O_{carb}$ varies from −14.6 to −0.3‰ VPDB and $\delta^{13}C_{carb}$ from −26 to −0.4‰ VPDB. The three abovementioned samples with carbonate content more than 5 wt.% demonstrate the highest $\delta^{18}O$ values within the section, close to 0‰, which is typical for sedimentary carbonates. Other samples with C_{carb} not exceeding 1 wt.% are essentially depleted in ^{18}O, and the $\delta^{13}C_{carb}$ values of these samples vary from −0.4 to −16.6‰. We suggest that the original isotopic composition, characteristic for sea water carbonates, was changed in carbonates of the investigated section in diagenesis and catagenesis, when the secondary carbonatization could take place at elevated temperatures in the presence of isotopically light CO_2 derived from the organic matter [55]. The layers with low carbonate content are mostly affected by secondary processes. One exception is the sample from member #8 with C_{carb} 9.9 wt.%, which, due to the low $\delta^{13}C$ value, −26‰, and high $\delta^{18}O$ value, −0.3‰, corresponds to sedimentary-diagenetic methane-derived limestones [56,57]. This type of carbonate with isotopically light carbon could be formed on the seabed in the areas of focused methane discharge under anaerobic conditions when methane, entering the bottom water, undergoes oxidation by microorganisms.

4.7. Integration of the Geochemical Data and Reconstruction of Sedimentation Conditions

Two genetically distinct groups of rocks were identified according to their geochemical features, they correspond to two sedimentation regimes. The first regime is characterized by noticeable input of biogenic material and pronounced marine organic matter accumulation in sediments, and another regime is associated with terrigenous sedimentation and mixed marine and terrigenous organic matter in rocks (Table 1, Figure A3).

Episodes of the increased role of biogenic sedimentation and organic matter accumulation occurred during the sea level transgression, the beginning of which was detected at the boundary of members #2 and #3 by the minimum content of terrigenous particles and the highest contribution of biogenic Si, S, P, Mg, and redox-sensitive metals. The peaks of biogenic sedimentation occur in members #3, #5, and #7. Their presence in the section in most cases correlates with episodes of anoxic environments characterized by Mo/(Mo+Mn) and V/Al, U, Th/U, Mo, and Mo/TOC [43,58–63]. The intervals are characterized by high TOC content, since a weak input of terrigenous material leads to the concentration of organic matter without its dilution.

The second series of rocks contain a significantly higher amount of the silt-clay component and could be distinguished by higher ratios of terrigenous elements Ti and Zi, Ti and Si, and Ti and K (Figure A3). Such rocks were formed during the enrichment of sediments with terrigenous material. Fluctuations in the terrigenous influx have determined the rate of organic matter accumulation and composition. In this section, we can assume the influence of more than two terrigenous sources. Starting from member #4, a new terrigenous source appears (different from that influenced members #1 and #2), and its influence is detected within the section up to member #8 by Ti/Zr and Rb/K, and $^{143}Nd/^{144}Nd$. Nd isotope ratio proves that the mineral part of members #1, #6, and #8 was significantly impacted by mineral component close in composition to the weathering crust of the Siberian platform.

Integrating all the factors, the studied section corresponds to an area with eustatic sea level changes during transgressive/regressive cycles and periodic activation of currents, supplying the sediments with terrigenous material and improving aeration of the bottom layers of the water column. The conclusion is consistent with the reported data on the paleogeography of the area in the Tithonian [3,64] (Figure 12). It was located in the isthmus between the Boreal Sea and the epicontinental Bazhenov Sea surrounded by Laurasia (modern Polar Urals and the Siberian Craton).

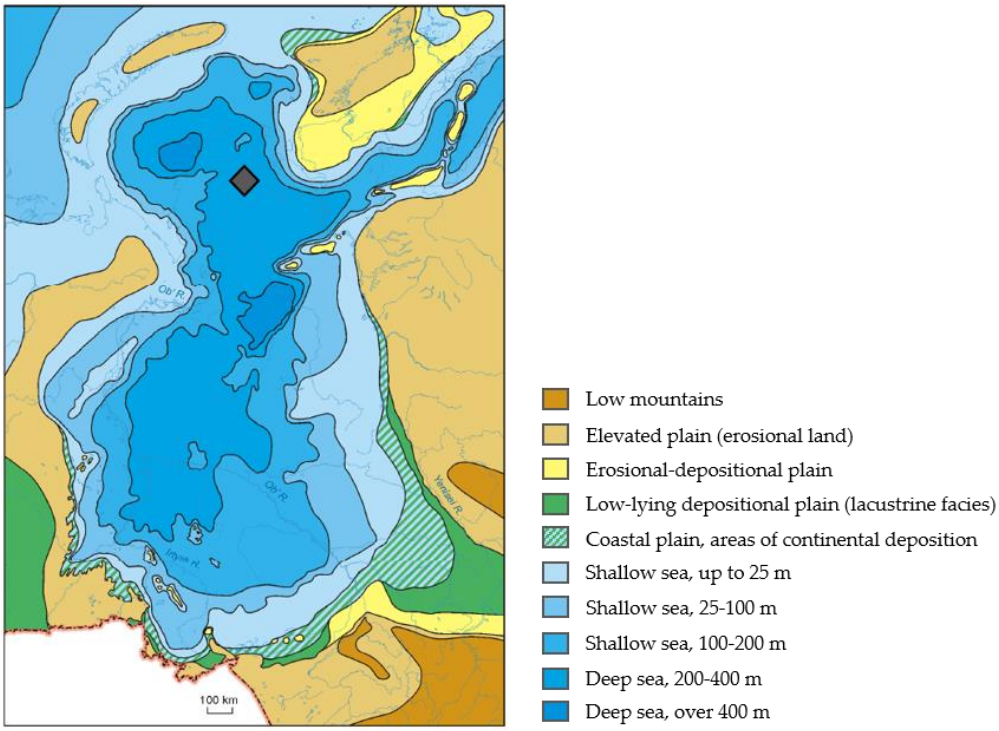
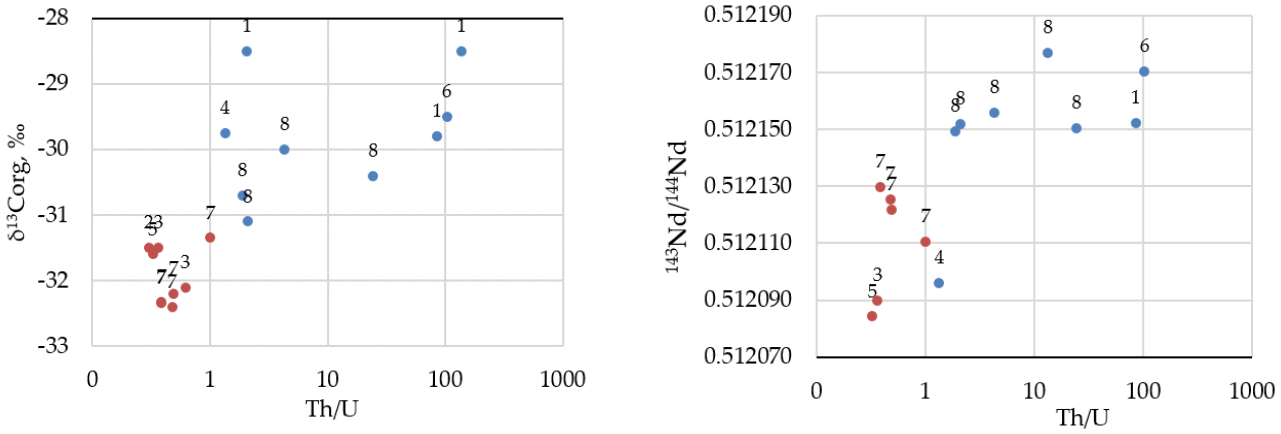


Figure 12. Paleogeography of the studied area (dark rhomb) in the Tithonian modified after Kontorovich [3].

Under the influence of the above discussed factors, including terrestrial influx and redox conditions, the amount and composition of organic matter in the members varies significantly (Figures 13 and 14).



(a) **(b)**

Figure 13. Relations between the Th/U ratio (logarithmic scale) and the isotope composition of organic matter (**a**) and Nd (**b**). The two series of samples represent TOC < 5 wt.% (blue) and TOC > 5 wt.% (red markers), and numbers correspond to geochemical members.

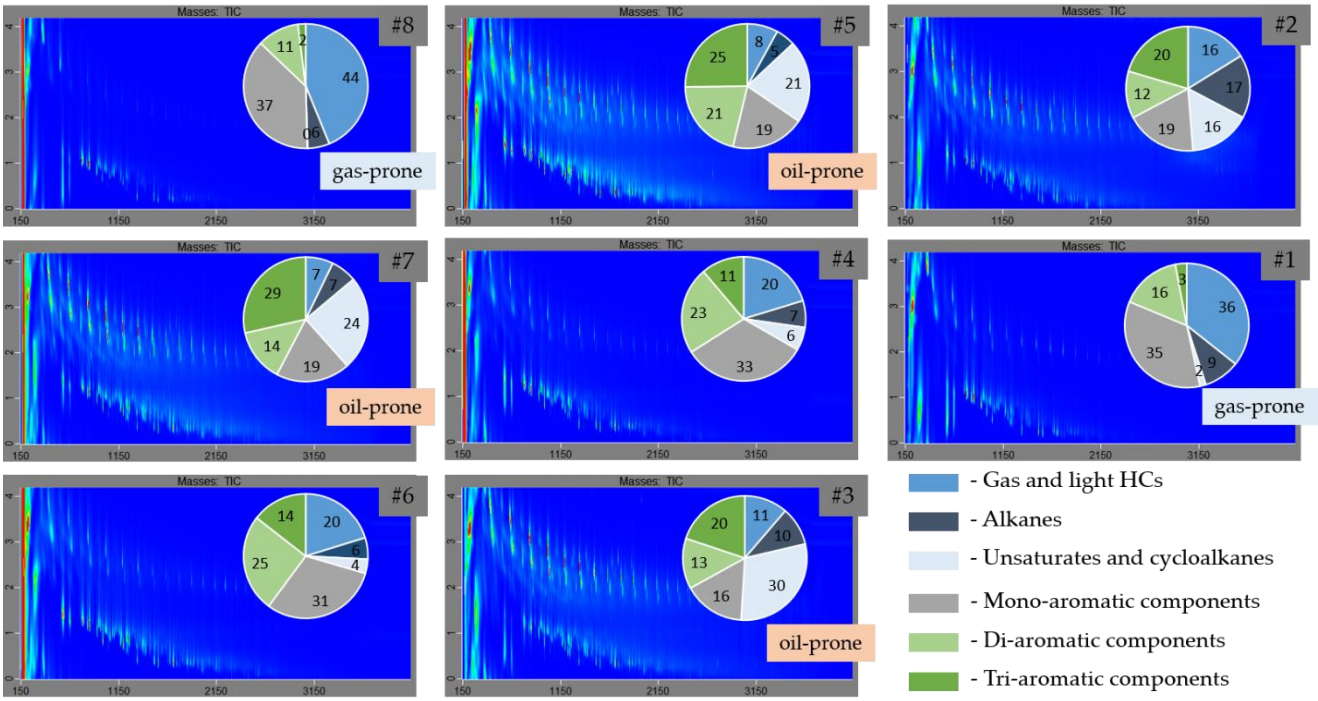


Figure 14. Kerogen cracking products distribution obtained at 500 °C and 0.5 min exposure time.

In members with mixed terrigenous and biogenic sedimentation (#3, #5, and #7) the accumulated TOC is higher than 5 wt.% in the vast majority of the samples. The rocks contain marine organic matter, represented by type II oil-prone kerogen. The hydrocarbon fluid characteristics are close to that of the sediments of the Bazhenov Formation in the central part of the Basin in terms of molecular, biomarker and isotopic composition (Figures 9b, 13 and 14) [9,49,50].

Organic matter in member #4 with average TOC = 4.3 wt.% is predominantly of marine origin, accumulated in more oxic conditions with a noticeable input of terrigenous material. Its transformation leads to the formation of oil and gas condensate, but the amount is lower compared to members #3, #5, and #7 (Figure 14).

The other members with average TOC < 5 wt.%, #1, #6, #8, were accumulated during periods of increased terrigenous influx and under oxic conditions. The terrigenous organic matter admixture is unambiguously identified by heavier C_{org} isotopic composition, only trace amounts of steranes, triaromatic steroids, and homohopanes, and C29/C30hop > 1 (in the case of interval #1, hopanes and steranes are absent). TOC in most samples does not exceed 4 wt.%, organic matter shows low GOC/TOC and HI, and high oxygen index (OI) = 19–26 mg CO_2/g TOC. Kerogen thermal decomposition products are mainly gas and heavy polyaromatic components.

For member #6, rocks are characterized by higher PI and extract composition, which is similar to the extracts of nearby kerogen-saturated rocks #5 and #7. These observations indicate better reservoir properties of the rocks from interval #6. The improved accumulating properties of the rock and the maturity of organic matter at the beginning of oil generation suggest the prospects for petroleum development. For other members with low TOC and a moderate to high proportion of terrigenous components (members #1, #2, #4, and #8), no reservoir properties were observed.

The main arguments in favor of the promising development of the studied area are high content of organic matter in the rock, a sufficient degree of maturity for kerogen conversion into mobile hydrocarbons, the presence of syngenetic mobile hydrocarbons in the section, and the alternation of intervals enriched with kerogen (and thus showing generating properties) with potentially accumulating intervals with increased reservoir properties.

5. Conclusions

In the Upper Jurassic–Lower Cretaceous section in the north of the West Siberian Petroleum Basin, we have identified eight geochemical members, which differ according to the elemental chemistry, amount and composition of organic matter. Using the geochemical and isotope data, we have performed a reconstruction of the depositional environment and evaluated the factors that have affected the distribution and composition of organic matter in the source rocks.

It was shown that the TOC content in the rocks is mainly controlled by the redox conditions and the intensity of terrigenous influx during sedimentation.

We attribute a simultaneous change in redox conditions and the intensity of terrigenous influx in the studied area to eustatic sea level changes during transgressive/regressive cycles and activation of currents. Transgression periods are associated with a weakened influence of terrigenous influx, low oxygenation with periodically expanded anoxia and intense accumulation and preservation of marine organic matter with oil-generating characteristics. The members #3, #5, and #7 were developed under such a depositional environment.

During eustatic regression periods, an increase in terrigenous influx and activation of currents in the studied area occurred simultaneously with an increase in oxygen, dissolved in water, and the proportion of terrigenous organic matter. In the lower part of the considered section, members #1 and #2 reflect these conditions. Starting from members #2 and #3, the periods of an intense accumulation of marine organic matter under reducing conditions were periodically changed to oxic environments with a more abundant terrigenous influx from another weathering source, which resulted in the fluctuations in organic matter content and composition. The generally moderate terrigenous inflow along the section is found increased for member #4, and to a greater extent for members #6 and #8. Under oxic conditions with the increased proportion of the terrigenous material, the formation of rocks depleted in organic matter, containing gas-generating kerogen, occurred (members #1, #2, #6, and #8).

The obtained results allowed us to evaluate the relationships between the sedimentation conditions and the petroleum generation characteristics of the current deposits. The paleoenvironment patterns, identified using a set of geochemical and isotopic methods, form the basis for the studies of different marine basins.

Using a set of geological, geochemical and isotopic methods, we have evaluated the relationships between paleo-sedimentation conditions, the composition of the source rocks and the petroleum generation characteristics of organic matter for the section of Bazhenov Formation in the north of the West Siberian Petroleum Basin. The identified paleoenvironment patterns contribute to the understanding of the Bazhenov unconventional resource formation and the prediction of hydrocarbon source and reservoir character in the time equivalent deposits in the region.

Author Contributions: Conceptualization, E.L., T.B., E.K., I.P., N.B., M.S.; methodology, E.K., T.K., A.V., I.P., Y.Y., E.L.; investigation, T.B., T.K., E.L., I.P., A.V., Y.Y.; resources, N.B. and E.K.; data curation, E.L., A.V., E.K., I.P.; writing—original draft preparation, E.L., I.P., A.V., M.S.; writing—review and editing, E.L., I.P., A.V., M.S., T.K., T.B.; visualization, E.L. and I.P.; supervision, M.S. and N.B.; project administration, N.B. and E.K.; funding acquisition, M.S. and N.B. All authors have read and agreed to the published version of the manuscript.

Funding: This work was supported by the Ministry of Science and Higher Education of the Russian Federation under agreement No. 075-10-2020-119 within the framework of the development program for a world-class Research Center.

Institutional Review Board Statement: Not applicable.

Informed Consent Statement: Not applicable.

Data Availability Statement: Data sharing not applicable.

Conflicts of Interest: The authors declare no conflict of interest.

Appendix A

Table A1. Summary of element composition measured by portable XRF-spectrometer.

Element, wt.%	Mg	Al	Si	P	S	K	Ca	Ti
Bazhenov Formation								
Min	0.31	1.50	3.61	0.00	0.94	0.35	0.75	0.00
Max	1.55	9.22	24.88	8.79	15.11	4.70	35.37	0.96
Average	1.10	7.96	21.12	0.32	3.96	3.70	3.22	0.74
Median	1.11	8.42	22.41	0.16	3.23	3.99	1.25	0.82
Abalak Formation								
Min	0.69	4.61	10.60	0.14	0.58	1.26	0.76	0.13
Max	1.34	8.93	25.07	0.25	2.79	4.65	4.46	1.01
Average	1.06	8.16	23.22	0.19	1.55	4.12	1.26	0.84
Median	1.06	8.33	23.89	0.19	1.51	4.28	1.03	0.87

Table A2. Summary of trace element composition measured by portable XRF-spectrometer.

Element, ppm	V	Ni	Cu	Zn	Rb	Sr	Zr	Mo	Ba
Bazhenov Formation									
Min	0	80	40	90	10	190	50	0	280
Max	4850	680	630	12460	330	3400	360	1250	2250
Average	890	280	290	2060	240	470	260	100	820
Median	0	250	240	1010	260	410	280	20	750
Abalak Formation									
Min	0	120	40	460	60	230	60	0	640
Max	0	550	250	2350	360	470	330	20	1530
Average	0	390	160	1530	300	420	280	0	1000
Median	0	380	160	1550	320	420	300	0	920

Table A3. Averaged pyrolysis parameters for 8 members.

Member #	Number of Samples Averaged	S0 + S1	S2	TOC	Tmax	HI	OI	PI	CC	GOC/ TOC
		mg HCs/g Rock	mg HCs/g Rock	wt.%	°C	mg HC/ g TOC	mg CO_2/ g TOC		wt.%	%
8	36	0.95	3.55	2.00	436	157	26	0.21	0.36	20
7	8	4.47	33.76	7.60	439	437	4	0.09	0.22	34
6	9	1.46	3.42	1.93	436	149	19	0.34	0.19	22
5	17	4.42	26.53	7.13	439	368	4	0.12	0.17	37
4	13	2.92	12.12	4.30	438	241	7	0.22	0.17	27
3	26	4.99	30.55	7.79	438	380	4	0.11	0.22	39
2	20	1.43	5.36	2.80	438	173	13	0.20	0.43	21
1	21	0.58	2.58	2.16	438	112	14	0.17	0.39	14

Table A4. Elemental and isotope composition of the rock samples.

Member #	C_{org}, wt.%	C_{carb}, wt.%	N, wt.%	S, wt.%	$\delta^{13}C_{org}$, ‰	$\delta^{34}S$, ‰	$\delta^{15}N$, ‰	$\delta^{13}C_{carb}$, ‰	$\delta^{18}O_{carb}$, ‰
8	1.92	9.93	0.06	0.23	−30.7	−30	7.4	−26	−0.3
	4.65	0.09	0.21	8.18	−31.1	−33.7	4.1	−12.9	−9.6
	3.40	0.19	0.2	4.13	−30.4	−30.9	3.8	−1.5	−5.4
	2.81	0.09	0.25	3.10	−30	−17.9	5.8	−12	−11.3
7	4.30	5.10	0.18	1.00	−32.4	−24.4	6.7	−5.5	−7.5
	8.80	0.42	0.33	4.98	−32.2	−33.7	4.8	−11.8	−10.1
	7.18	0.83	0.23	1.48	−32.3	−25.8	6.0	−0.4	−5.9
	8.17	0.27	0.27	1.86	−32.3	−27.9	5.9	−13.8	−14.6
	7.58	0.02	0.28	2.65	−31.4	−34.7	4.8	−13.9	−13.8
6	1.01	0.19	0.13	3.20	−29.5	−7.8	7.3	−14.1	−12.1
5	9.53	0.32	0.36	2.76	−31.6	−29.3	4.2	−10.5	−8.4
4	2.08	0.22	0.16	4.00	−29.8	−30.0	7.0	−16.6	−13.6
3	7.80	0.06	0.29	2.00	−31.5	−32.4	3.2	−15.5	−12.1
	6.00	0.46	0.25	4.44	−32.1	−36.6	2.5	−15.6	−13.1
	11.13	0.27	0.38	7.70	−31.5	−37.3	4.1	−15.1	−12.6
2	1.48	0.36	0.15	5.85	−28.5	−24.1	5.9	−15.9	−10.7
1	2.65	0.28	0.18	3.19	−29.8	−20.4	3.8	−15.3	−12.2
	0.56	8.06	0.05	0.36	−28.5	−18.6	9.8	−10.8	−1.2

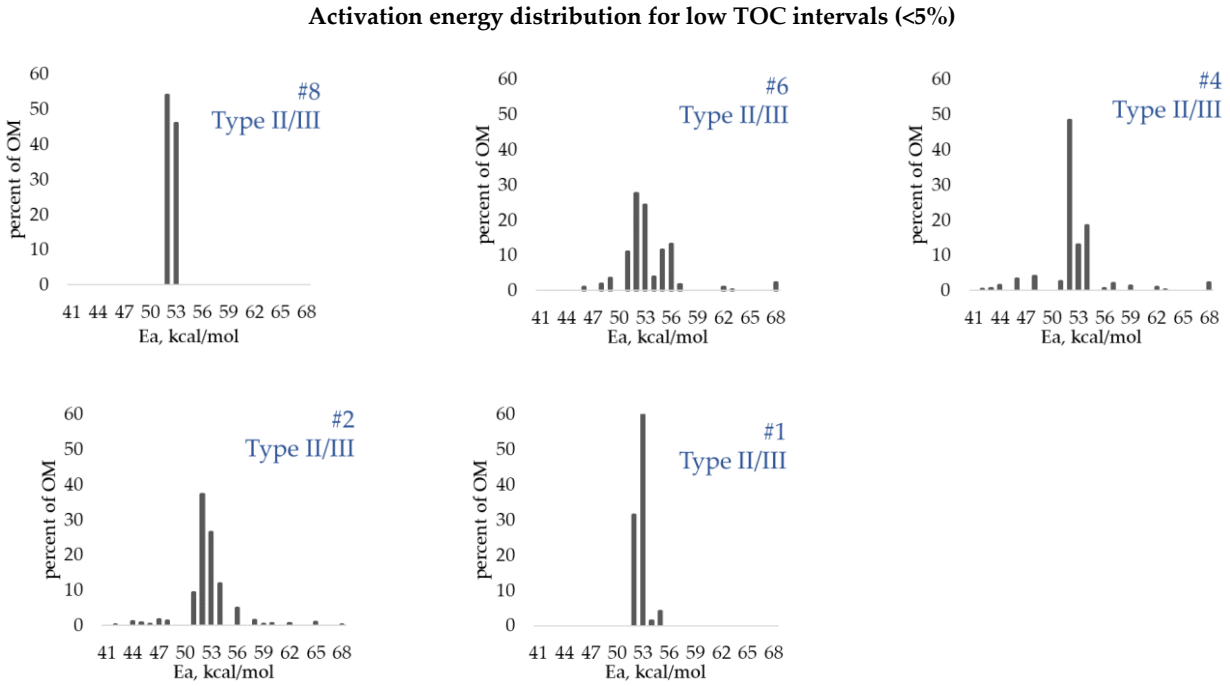


Figure A1. Representative bulk kinetic spectra (A = $1 \cdot 10^{14}$ s^{-1}) of kerogen decomposition for low TOC members #1, #2, #4, #6, #8.

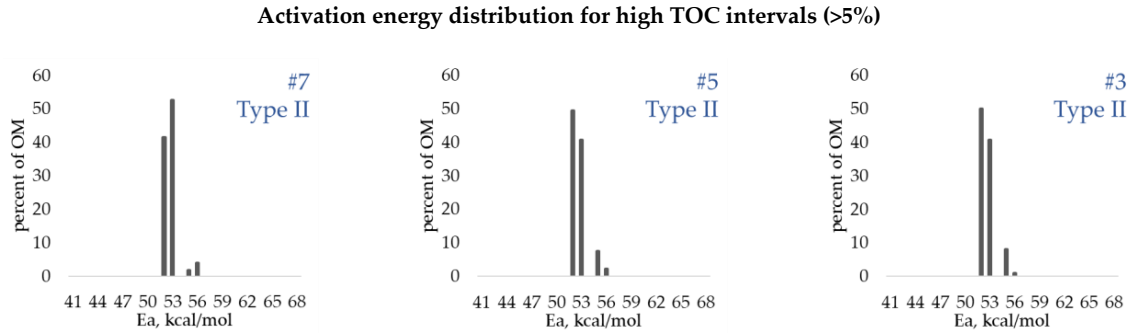


Figure A2. Representative bulk kinetic spectra (A = 1 × 10^{14} s^{-1}) of kerogen decomposition for high TOC members #3, #5, and #7.

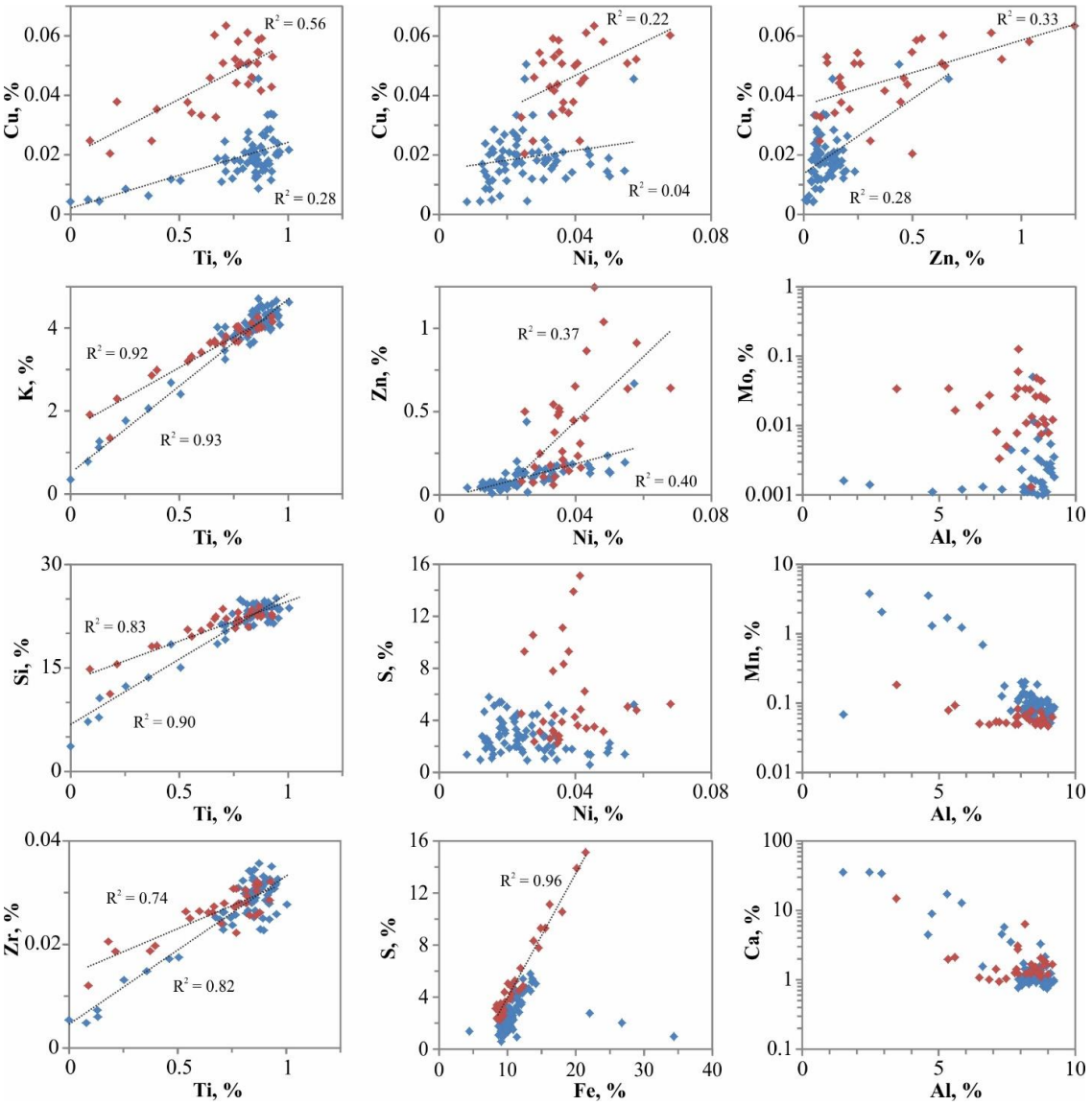


Figure A3. Cross-plots of element content in rocks. The two series of samples represent deposits of different genesis: terrigenous with the increased role of biogenic sedimentation (members #3, #4, #5, and #7, red markers) and predominantly terrigenous sedimentation (members #1, #2, #6, and #8, blue markers). The correlations are drawn where found, and correlation factor is given (R^2).

References

1. Braduchan, Y.V.; Gurari, F.G.; Zakharov, V.A. *Bazhenovskij Gorizont Zapadnoj Sibiri (Stratigrafija, Ekosistema, Neftenosnost) (The Bazhenov Horizon of the Western Siberia (Stratigraphy, Ecosystem, Oil Content)*; Vyshemiskij, V.S., Ed.; Nauka: Novosibirsk, Russia, 1986.
2. Kontorovich, A.E.; Bogorodskaya, L.I.; Borisova, L.S.; Burshtein, L.M.; Ismagilov, Z.R.; Efimova, O.S.; Kostyreva, E.A.; Lemina, N.M.; Ryzhkova, S.V.; Sozinov, S.A.; et al. Geochemistry and catagenetic transformation of kerogen from the bazhenov horizon. *Geoshemistry* **2019**, *64*, 585–593. [CrossRef]
3. Kontorovich, A.E.; Kontorovich, V.A.; Ryzhkova, S.V.; Shurygin, B.N.; Vakulenko, L.G.; Gaideburova, E.A.; Danilova, V.P.; Kazanenkov, V.A.; Kim, N.S.; Kostyreva, E.A.; et al. Jurassic paleogeography of the West Siberian sedimentary basin. *Russ. Geol. Geophys.* **2013**, *54*, 747–779. [CrossRef]
4. Zanin, Y.N.; Zamirailova, A.G.; Eder, V.G. Some aspects of the Bazhenov Formation genesis in the Central parts of the West-Siberian sedimentary Basin. *Lithosphera* **2005**, *4*, 118–135.
5. Ulmishek, G.F. *Petroleum Geology and Resources of the West. Siberian Basin, Russia*, 1st ed.; US Geological Survey: Reston, VA, USA, 2003.
6. Zubkov, M.Y. The reservoir potential of the Bazhenov Formation: Regional prediction. *Russ. Geol. Geophys.* **2017**, *58*, 410–415. [CrossRef]
7. Goncharov, I.V.; Samoilenko, V.V.; Oblasov, N.V.; Fadeeva, S.V.; Veklich, M.A.; Kashapov, R.S.; Trushkov, P.V.; Bahtina, E.S. Types of organic matter and catagenesis of the Bazhenov formation and its same-aged analogues. *Oil Ind.* **2016**, *10*, 20–25.
8. Zanin, Y.N.; Zamirailova, A.G.; Eder, V.G. Uranium, thorium, and potassium in black shales of the Bazhenov Formation of the West Siberian marine basin. *Lithol. Miner. Resour.* **2016**, *51*, 74–85. [CrossRef]
9. Kostyreva, E.A.; Sotnich, I.S. Geochemistry of organic matter of the Bazhenov Formation in the north of the Khantei anteclise. *Russ. Geol. Geophys.* **2017**, *58*, 434–442. [CrossRef]
10. Goncharov, I.V.; Samoilenko, V.V.; van Graas, G.W.; Trushkov, P.V.; Oblasov, N.V.; Fadeeva, S.V.; Veklich, M.A.; Kashapov, R.S.; Sidorov, D.A. Petroleum generation and migration in the southern Tyumen region, Western Siberia Basin, Russia. *Org. Geochem.* **2021**, *152*, 104178. [CrossRef]
11. Toropova, T.N.; Kontorovich, V.A. Structural history and petroleum potential of the Central part of the Gydan Peninsula (Northeast of Western Siberia). *Neftegazov. Geol. Teor. Pract.* **2019**, *14*, 1–25. [CrossRef]
12. Deshin, A.A.; Safronov, P.I.; Burshtein, L.M. Reconstruction of hydrocarbon generation and accumulation on the Gydan Peninsula and adjacent offshore areas using basin modeling approach. *IOP Conf. Ser. Earth Environ. Sci.* **2018**, *193*. [CrossRef]
13. Ryzhkova, S.V.; Burshtein, L.M.; Ershov, S.V.; Kazanenkov, V.A.; Kontorovich, A.E.; Kontorovich, V.A.; Nekhaev, A.Y.; Nikitenko, B.L.; Fomin, M.A.; Shurygin, B.N.; et al. The Bazhenov Horizon of West Siberia: Structure, Correlation, and Thickness. *Russ. Geol. Geophys.* **2018**, *59*, 1053–1074. [CrossRef]
14. Afanasenkov, A.P.; Petrov, A.L.; Grayzer, E.M. Geochemical description and oil & gas generation potential of Mesozoic formations within the Gydan and Yenisei-Khatanga oil and gas bearing regions. *Oil Gas Geol.* **2018**, 109–127. [CrossRef]
15. Skorobogatov, V.A.; Stroganov, L.V. *Gydan Region: Geological Structure, Hydrocarbon Resources, Future*; NEDRA: Moscow, Russia, 2006; ISBN 5836502625.
16. Fjellanger, E.; Kontorovich, A.E.; Barboza, S.A.; Burshtein, L.M.; Hardy, M.J.; Livshits, V.R. Charging the giant gas fields of the NW Siberia basin. *Pet. Geol. Conf. Proc.* **2010**, *7*, 659–668. [CrossRef]
17. Kontorovich, A.E.; Burshtein, L.M.; Malyshev, N.A.; Safronov, P.I.; Gus'kov, S.A.; Ershov, S.V.; Kazanenkov, V.A.; Kim, N.S.; Kontorovich, V.A.; Kostyreva, E.A.; et al. Historical-geological modeling of hydrocarbon generation in the Mesozoic-Cenozoic sedimentary basin of the Kara Sea (basin modeling). *Russ. Geol. Geophys.* **2013**, *54*, 917–957. [CrossRef]
18. Kontorovich, A.E.; Burshtein, L.M.; Nikitenko, B.L.; Ryzhkova, S.V.; Borisov, E.V.; Ershov, S.V.; Kostyreva, E.A.; Konotorovich, V.A.; Nekhaev, A.Y.; Ponomareva, E.V.; et al. Volgian–early berriasian marginal filter in the West Siberian marine basin and its influence on sediment distribution. *Russ. Geol. Geophys.* **2017**, *58*, 410–415. [CrossRef]
19. Polyakova, I.D.; Bogoyavlenskii, V.I. The Bazhenovo formation as a source of economic oils and rich gases in the Tithonian-Neocomian section of the South Kara Region. *Dokl. Earth Sci.* **2011**, *440*, 1270–1275. [CrossRef]
20. Katz, B.J.; Robison, C.R.; Chakhmakhchev, A. Aspects of hydrocarbon charge of the petroleum system of the Yamal Peninsula, West Siberia basin. *Int. J. Coal Geol.* **2003**, *54*, 155–164. [CrossRef]
21. Samoilenko, V.V.; Shadrina, E.S.; Goncharov, I.V.; Oblasov, N.V.; Veklich, M.A.; Zherdeva, A.V. The Origin of Hydrocarbon Fluids and Features of the Formation of Oil and Gas Fields in the Gydan Peninsula. In Proceedings of the 29th International Meeting on Organic Geochemistry, European Association of Geoscientists & Engineers, Gothenburg, Sweden, 1–6 September 2019; Volume 2019, pp. 1–2.
22. Chakhmakhchev, A.; Sampei, Y.; Suzuki, N. Geochemical characteristics of oils and source rocks in the Yamal peninsula, West Siberia, Russia. *Org. Geochem.* **1994**, *22*, 311–322. [CrossRef]
23. Panchenko, I.V.; Nemova, V.D.; Smirnova, M.E.; Ilyina, M.V.; Baraboshkin, E.Y.; Ilyin, V.S. Stratification and detailed correlation of Bazhenov Horizon in the central part of the Wetern Siberia according to lithological and paleontological core analysis and well logging. *Oil Gas Geol.* **2016**, *6*, 22–34.
24. Kontorovich, A.E.; Yan, P.A.; Zamirailova, A.G.; Kostyreva, E.A.; Eder, V.G. Classification of rocks of the Bazhenov Formation. *Russ. Geol. Geophys.* **2016**, *57*, 1606–1612. [CrossRef]

25. Zakharov, V.A. Formation conditions of the Volgian-Berrias carbon-rich Bazhenovov Formation based on paleoecology data. *Evol. Biosf. Bioraznoobrazija* **2006**, *5*, 552–568.
26. Zubkov, M.Y. Rocks of the Bazhenovo and Abalak formations, Central Krasnoleninsk arch, Western Siberia: Composition, structure, and formation conditions. *Lithol. Miner. Resour.* **2001**, *36*, 33–42. [CrossRef]
27. Bychkov, A.Y.; Kalmykov, G.A.; Bugaev, I.A.; Balushkina, N.S.; Kalmykov, A.G. The geochemical patterns of rocks of the Bazhenov and Abalak formations (Western Siberia). *Moscow Univ. Geol. Bull.* **2017**, *72*, 87–94. [CrossRef]
28. Skvortsov, M.B.; Nemova, V.D.; Panchenko, I.V.; Kirsanov, A.M. Criteria of oil bearing capacity of the Bazhenov formations. *Oil Gas Geol.* **2018**, *1*, 109–114.
29. Practical Steps for Studying Mudstones in Thin Sections. In *Mudstone Primer: Lithofacies Variations, Diagnostic Criteria, and Sedimentologic–Stratigraphic Implications at Lamina to Bedset Scale*; Lazar, O.R.; Bohacs, K.M.; Schieber, J.; Macquaker, J.H.S.; Demko, T.M. (Eds.) SEPM Society for Sedimentary Geology: Tulsa, OK, USA, 2015; Volume 12, ISBN 9781565763395.
30. Panchenko, I.; Kulikov, P.; Garipov, R. Practical application of chemostratigraphy and lithochemistry methods in the study of oil bearing black shale. In Proceedings of the EAGE/SPE Workshop on Shale Science 2021, Moscow, Russia, 5–6 April 2021; pp. 1–5. [CrossRef]
31. Espitalie, J.; Laporte, J.L.; Madec, M.; Marquis, F.; Leplat, P.; Paulet, J.; Boutefeu, A. Methode rapide de caracterisation des roches meres, de leur potential Per., petrolier et de leur degre d'evolution. *Rev. Inst. Fr. Pét.* **1977**, *32*, 23–42. [CrossRef]
32. Espitalié, J.; Deroo, G.; Marquis, F. La pyrolyse Rock Eval et ses applications. *Rev. Inst. Fr. Pét.* **1985**, *40*, 755–784. [CrossRef]
33. Umamaheswaran, R.; Prasad, G.V.R.; Rudra, A.; Dutta, S. Biomarker signatures in triassic coprolites. *Palaios* **2019**, *34*, 458–467. [CrossRef]
34. Li, S.; Cao, J.; Hu, S.; Zhang, D.; Fan, R. Analysis of terpanes in biodegraded oils from China using comprehensive two-dimensional gas chromatography with time-of-flight mass spectrometry. *Fuel* **2014**, *133*, 153–162. [CrossRef]
35. Li, S.; Cao, J.; Hu, S. Analyzing hydrocarbon fractions in crude oils by two-dimensional gas chromatography/time-of-flight mass spectrometry under reversed-phase column system. *Fuel* **2015**, *158*, 191–199. [CrossRef]
36. Lazar, O.R.; Bohacs, K.M.; Macquaker, J.H.S.; Schieber, J.; Demko, T.M. Capturing key attributes of fine-grained sedimentary rocks in outcrops, cores, and thin sections: Nomenclature and description guidelines. *J. Sediment. Res.* **2015**, *85*, 230–246. [CrossRef]
37. Mukhametdinova, A.; Karamov, T.; Bogdanovich, N.; Borisenko, S.; Rudakovskaya, S.; Cheremisin, A. Wettability of organic-rich source rocks: Case study on Bazhenov Formation (Abalak-Bazhenov group). *Adv. Geosci.* **2020**, *54*, 195–204. [CrossRef]
38. Yudovich, Y.E.; Ketris, M.P. *Geokhimiya Chernykh Slantsev (Geochemistry of Black Shales)*; Nauka: Leningrad, Russia, 1988.
39. Yudovich, Y.E.; Ketris, M.P. *Osnovy Litokhimii (Fundamentals of Lithochemistry)*; Nauka: St.Petersburg, Russia, 2000.
40. Barash, I.G.; Bulanov, V.A.; Gladkochub, D.P.; Donskaya, T.V.; Ivanov, A.V.; Letnikova, E.F.; Mironov, A.G.; Sizykh, A.I.; Sklyarov, E.V. *Interpretatsiya Geokhimicheskikh Dannykh/Uchebnoe Posobie*; Sklyarov, B.V., Ed.; Intermetinzhiniring: Moscow, Russia, 2001.
41. Maslov, A.V. *Osadochnye Porody: Metody Izucheniya i Interpretatsii Poluchennykh Dannykh. Uchebnoe Posobie (Sedimentary Rocks: Methods for the Interpretation of Obtained Data. A Manual)*; UGGU: Yekaterinburg, Russia, 2005.
42. Ratcliffe, K.T.; Woods, J.; Rice, C. Determining well-bore pathways during multilateral drilling campaigns in shale resource plays: An example using chemostratigraphy from hte Horn River Formation, British Columbia, Canada. In Proceedings of the Eastern Australia Basins Symposium IV, Brisbane, QLD, Australia, 10–14 September 2012; pp. 143–148.
43. Algeo, T.J.; Li, C. Redox classification and calibration of redox thresholds in sedimentary systems. *Geochim. Cosmochim. Acta* **2020**, *287*, 8–26. [CrossRef]
44. Ruebsam, W.; Dickson, A.J.; Hoyer, E.-M.; Schwark, L. Multiproxy reconstruction of oceanographic conditions in the southern epeiric Kupferschiefer Sea (Late Permian) based on redox-sensitive trace elements, molybdenum isotopes and biomarkers. *Gondwana Res.* **2017**, *44*, 205–218. [CrossRef]
45. Andersson, P.; Guo, L.; Semiletov, I.; Gustafsson, O.; Ingri, J.; Dudarev, O.; White, D. Nd and Sr isotopes in Siberian Arctic estuarine sediments: Implications for sediment provenance (5475). In Proceedings of the EGS-AGU-EUG Joint Assembly, Nice, France, 6–11 April 2003.
46. Asadulin, E.E.; Miroshnikov, A.Y.; Velichkin, V.I. Geochemical signature of bottom sediments in the mixing zones of Ob and Yenisei waters with Kara Sea water. *Geochem. Int.* **2013**, *51*, 1005–1018. [CrossRef]
47. Bjoroy, M.; Hall, K.; Hall, P.B. Detailed hydrocarbon analyser for well site and laboratory use. *Mar. Pet. Geol.* **1992**, *9*, 648–665. [CrossRef]
48. Hall, P.B.; Stoddart, D.; Bjorøy, M.; Larter, S.R.; Brasher, J.E. Detection of petroleum heterogeneity in Eldfisk and satellite fields using thermal extraction, pyrolysis-GC, GC-MS and isotope techniques. *Org. Geochem.* **1994**, *22*, 383–402. [CrossRef]
49. Peters, K.E.; Kontorovich, A.E.; Moldowan, J.M.; Andrusevich, V.E.; Huizinga, B.J.; Demison, G.J.; Stasova, O.F. Geochemistry of selected oils and rocks from the central portion of the West Siberian Basin, Russia. *Am. Assoc. Pet. Geol. Bull.* **1993**, *77*, 863–887. [CrossRef]
50. Liu, Z.; Moldowan, J.M.; Nemchenko-Rovenskaya, A.; Peters, K.E. Oil families and mixed oil of the North-Central West Siberian basin, Russia. *Am. Assoc. Pet. Geol. Bull.* **2016**, *100*, 319–343. [CrossRef]
51. Peters, K.E.; Walters, C.C.; Moldowan, J.M. *The Biomarker Guide: Volume 2, Biomarkers and Isotopes in Petroleum Exploration and Earth History*; Cambridge University Press: Cambridge, UK, 2005.
52. Kontorovich, A.E.; Kostyreva, E.A.; Melenevskij, V.N.; Moskvin, V.I.; Fomin, A.N. Geochemical criteria of oil and gas prospects for Mezozoic deposits of the South-Eatern Siberia. *Geol. Neft. Gaza* **2009**, *1*, 4–12.

53. Newton, R. Water Column Redox Proxies. School of Earth and Environment. Available online: http://www.lifeandplanet.net/uploads/8/6/7/2/8672988/newton_-_water_column_redox_edited.pdf (accessed on 5 May 2021).
54. Sim, M.S.; Bosak, T.; Ono, S. Large Sulfur isotope fractionation does not require disproportionation. *Science* **2011**, *333*, 74–77. [CrossRef]
55. Yurchenko, A.; Voropaev, A.; Kozlova, E.; Morozov, N.; Spasennykh, M. Application of the data on δ13C and δ18O of carbonates for the study of unconventional reservoirs on the example of the Bazhenov source rocks, Western Siberia, Russia. *Geosciences* **2021**, *11*, 264. [CrossRef]
56. Yurchenko, A.Y. Genesis of calcite in carbonates within sedimentary basins according to carbon and oxygen stable isotopes distribution. *Moscow Univ. Geol. Bull.* **2014**, 107–110. [CrossRef]
57. Yurchenko, A.Y.; Balushkina, N.S.; Kalmykov, G.A.; Shardanova, T.A.; Bychkov, A.Y.; Prokof'ev, V.Y. Genesis of vein calcite in carbonate rocks at top of Abalak and Georgiev formations in Central West Siberia. *Oil Ind.* **2015**, *4*, 22–26.
58. Lewan, M.D. Factors controlling the proportionality of vanadium to nickel in crude oils. *Geochim. Cosmochim. Acta* **1984**, *48*, 2231–2238. [CrossRef]
59. Jones, B.; Manning, D.A.C. Comparison of geochemical indices used for the interpretation of palaeoredox conditions in ancient mudstones. *Chem. Geol.* **1994**, *111*, 111–129. [CrossRef]
60. Tribovillard, N.; Algeo, T.J.; Lyons, T.; Riboulleau, A. Trace metals as paleoredox and paleoproductivity proxies: An update. *Chem. Geol.* **2006**, *232*, 12–32. [CrossRef]
61. Algeo, T.J.; Rowe, H. Paleoceanographic applications of trace-metal concentration data. *Chem. Geol.* **2012**, *324–325*, 6–18. [CrossRef]
62. Algeo, T.J.; Liu, J. A re-assessment of elemental proxies for paleoredox analysis. *Chem. Geol.* **2020**, *540*, 119549. [CrossRef]
63. Bennett, W.W.; Canfield, D.E. Redox-sensitive trace metals as paleoredox proxies: A review and analysis of data from modern sediments. *Earth-Sci. Rev.* **2020**, *204*, 103175. [CrossRef]
64. Shemin, G.; Deev, E.; Vernikovsky, V.A.; Drachev, S.S.; Moskvin, V.; Vakulenko, L.; Pervukhina, N.; Sapyanik, V. Jurassic paleogeography and sedimentation in the northern West Siberia and South Kara Sea, Russian Arctic and Subarctic. *Mar. Pet. Geol.* **2019**, *104*, 286–312. [CrossRef]